our future through science

The Elandskraal Fire, Knysna

A data driven analysis


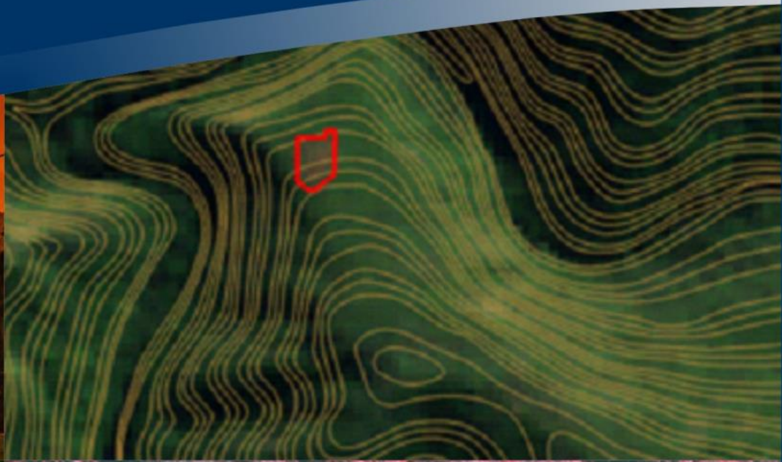
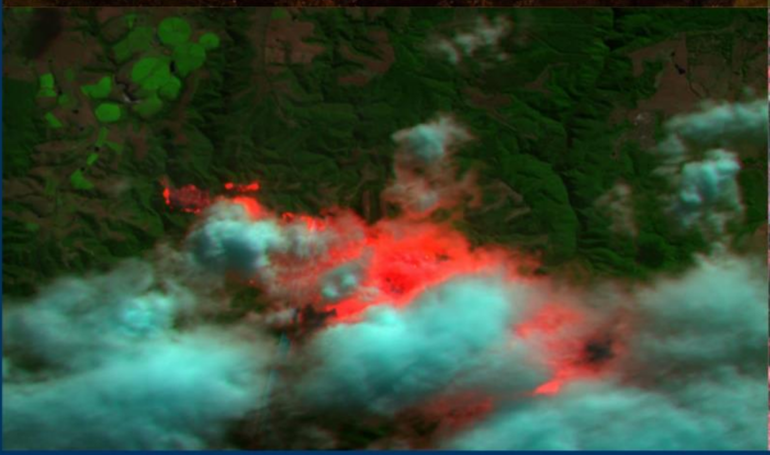


The Elandskraal Fire, Knysna

A data driven analysis

June 2018

Authors: PE Frost[1], LG Kleyn[1], R van den Dool[1], M Burgess[1], L Vhengani[1], K Steenkamp[1], K Wessels[1]

Internal reviewers: DC Le Maitre[2], GG Forsyth[2]

[1]CSIR Meraka Institute
[2]CSIR Natural Resource and Environment

CSIR
our future through science

Contact: Philip Frost

CSIR Meraka Institute,

Meiring Naude Rd, Brummeria, South Africa

Email: pfrost@csir.co.za

CSIR Report number: 271960-1

Disclaimer: This report represents the opinion of the researchers who compiled it in good faith, based on data which is believed to be true and reliable at the time of publication. CSIR hereby disclaims all warranties, implied or expressed, relating to the report, regardless of form, and related documentation including warranties of non-infringement, quality and accuracy, fitness of a particular purpose and timeliness of the data. Use of the report and any data or conclusions contained therein is entirely at the user's risk.

CONTENTS

EXECUTIVE SUMMARY 5

1 INTRODUCTION 8

2 STUDY AREA 10

3 TIMELINE OF EVENTS 12

4 DETAILED TECHNICAL ANALYSIS 14

4.1 SENSORS AND DATA 14

4.2 BEFORE THE FIRE 18

4.2.1 Drought and vegetation condition 18
4.2.2 Vegetation type 19
4.2.3 Smouldering vegetation 20
4.2.4 Lightning as a potential source of ignition 27
4.2.5 "Holdover" fires 30
4.2.6 Weather before the fire 31

4.3 START OF THE FIRE 32

4.3.1 Weather on 7 June 2017 32
4.3.2 First detection of the Elandskraal fire 34

4.4 INITIAL SPREAD OF THE FIRE 37

4.4.1 Spread to Kooigoed 39
4.4.2 Estimated rate of spread 40
4.4.3 Rothermel fire spread model simulation 42
4.4.4 Influence of topography 44
4.4.5 Spotting 45

4.5 AFTER THE FIRE 46

4.5.1 Activation of the International Charter for Space and Major Disasters 46
4.5.2 Total burned area 46

5 SUMMARY AND CONCLUSIONS 48

6 RECOMMENDATIONS 52

7 ACKNOWLEDGEMENTS 53

8 REFERENCES 54

9 GLOSSARY 58

TABLES

Table 1. List of sensors used in analyses along with their sources and details of date and time of acquisition. (details of sensors are available by following the provided hyperlinks) 17

FIGURES

Figure 1. Active fires detected by MODIS and VIIRS satellite sensors on 7-8 June 2017 displayed in the online viewer of the Advanced Fire Information System (AFIS). 9

Figure 2. (A) Overview of the greater Knysna region of South Africa, indicating the burned area (dark grey) of the Uniondale, Elandskraal and Kruisfontein fires. (B) The burned area of the Elandskraal and Kruisfontein fires in shades of pink amongst the green unburned vegetation in the Sentinel-2 satellite image (14 June 2017). (C) WorldView-3 image (19 June 2017) of the probable origin of Elandskraal fire showing burned vegetation and the location of the “holdover” fire and the weather station at Kooigoed. 11

Figure 3. A timeline of diverse datasets used in the analysis of the Elandskraal fire from 19 March to 19 June 2017. 14

Figure 4. Minimum size of fire (ha) that can be detected by SEVIRI sensor on MSG satellite, at different fire temperatures and latitudes, taking atmospheric attenuation into account (from Calle *et al*. 2006). For the Elandskraal latitude of 34°, the range between 20° and 50° latitude where used where the thermal gradient of 6K/15 minutes is applicable to night time atmospheric attenuation. 16

Figure 5: Garden Route Dam level from 2014 to 2017: National Integrated Water Information System (NIWIS). 18

Figure 6: The long-term mean EVI (red) compared to 2016 (light grey) and 2017 (brown) of the 3 300 ha burned area in the Elandskraal. The EVI of 2010 provides a reference for very dry conditions (dark grey). 19

Figure 7: Drone footage taken on 27 May 2017 showing a smouldering patch of brown vegetation in the north-west corner of Elandskraal along the Karatara River (33.957624 S, 22.839807 E). 20

Figure 8: Visible evidence of brown vegetation in the GeoEye-1 satellite image of 20 April 2017 displayed in Google Earth (33.957624 S, 22.839807 E). 21

Figure 9a: Enhanced Vegetation Index (EVI) of Sentinel-2 imagery of 19 March 2017. The vegetation at the location of the subsequently identified smouldering patch has EVI values greater than 0.4 which is an indicator of healthy vegetation. 22

Figure 9b: Enhanced Vegetation Index (EVI) of Sentinel-2 imagery of 29 March 2017. EVI values have decreased from 0.41 to 0.32. A decrease in greenness is an indicator of vegetation stress as depicted in the inset map, where brown = decrease and green = increase in vegetation greenness between the 19 and 29 March 2017. 22

Figure 9c: Enhanced Vegetation Index (EVI) of Sentinel-2 imagery of 8 April 2017 where the pixel EVI values have decreased by 17% and the size of the vegetation anomaly has increased. A decrease in greenness is an indicator of vegetation stress as depicted in the inset map, where brown = decrease and green = increase in vegetation greenness between the 19 March and 8 April 2017. 23

Figure 9d: Enhanced Vegetation Index (EVI) of Sentinel-2 imagery of 5 May 2017 where the pixel EVI values have dropped to 0.28 and the size of the anomaly has increased. A decrease in greenness is an indicator of vegetation stress as depicted in the inset map, where brown = decrease and green = increase in vegetation greenness between the 19 March and 5 May 2017. 24

Figure 9e: Enhanced Vegetation Index (EVI) of Sentinel-2 imagery of 18 May 2017 where the pixel EVI values have stabilised at 0.28 but the size of the vegetation anomaly has increased to 3 033 m^2. A decrease in greenness is an indicator of vegetation stress as depicted in the inset map, where brown = decrease and green = increase in vegetation greenness between the 19 March and 18 May 2017. 24

Figure 10. Area of vegetation affected by the smouldering fire at Elandskraal from 19 March to 18 May 2017, including the estimated area by 27 May and 6 June based on the average rate of growth of 50 m^2/day. The average Enhanced Vegetation Index (EVI) of all pixels within the growing smouldering area (green line). 25

Figure 11: Spatial expansion of the smouldering patch of vegetation according to Sentinel-2 imagery and the estimate for the continued expansion between 27 May and 6 June based on the average rate of expansion. Background image is Sentinel-2 EVI of 18 May 2017. 26

Figure 12: The expansion of the vegetation anomaly (Figure 11) for different Sentinel-2 dates (green = 29/03/2017; pink = 8/4/2017; purple = 5/5/2017; olive green = 18/5/2017) with a background image of the WorldView-3 image of 19 June 2017 showing the Elandskraal burned area after the fire. 26

Figure 13: Centroids of estimated locations of lightning strike (99% confidence ellipses) as detected by the SAWS SALDN for period 1 Jan 2017 - 7 June 2017 around Elandskraal. The colours of the points indicate the polarity of the strike and the dates before or after 29 March 2017 (when the vegetation anomaly was detected). 27

Figure 14: Positive lightning strike ellipses with a 99% confidence level for greater Knysna region and Elandskraal area between 1 Jan 2017 and 29 March 2017. 28

Figure 15: Positive lightning strike ellipses with a 99% confidence level area for 18 February and 22 March 2017 in relation to the site of smouldering vegetation in Elandskraal area. 29

Figure 16: Location of smouldering patch of vegetation (yellow) within the 99% confidence ellipse (red) of the 22 March 2017, provided by SAWS. 30

Figure 17: Lowveld Fire Danger Index (LFDI) at Kooigoed weather station (33.9628 S, 22.855 E) from 29 May 2017 to 7 June 2017. 32

Figure 18: Weather parameters as measured on 7 June 2017 by Kooigoed weather station located 1.4 km south-east of the holdover fire (33.963 S, 22.855 E). Red vertical lines indicate significant changes in weather conditions. 33

Figure 19. Timeline of active fire detections by satellite sensors and Bushnell motion-sensing camera on 7 June 2017. 34

Figure 20. NPP VIIRS Day-Night band showing fire near Uniondale at 01h10 on 7 June but no detectable fire at Elandskraal. 35

Figure 21. Radiance of active fires detected by MSG satellite in the early hours of 7 June 2017 showing the sequence of fire spread. 36

Figure 22. The croquet lawn, circled in red, with wind direction at 05h00 indicated by white arrows. 37

Figure 23. The burn scar visible on the croquet lawn as observed by drone footage on 8 June 2017 affected from the north-west . 38

Figure 24. The WorldView-3 burned area imagery used to confirm that the north-westerly wind would affect the burn pattern on the croquet field as shown. 38

Figure 25. Photographs captured by Bushnell motion-sensing camera at Kooigoed triggered at a) 06h48, b) 06h50 and c) 06h52 on the morning of the 7 June 2017. 40

Figure 26. Distances between relevant points in the burned area showing the estimated 1-2 ha fire registered by the MSG satellite (dark blue polygon) at 06h03. Burned area (light blue shades outlined in yellow) was mapped with WorldView-3. 41

Figure 27. Rothermel Fire Spread Model output based on the starting point at the location of the holdover fire, topography and average weather station data from 05h01, 05h06, 05h12 and 05h17 (RH% = 36; Ave Wind Speed = 23 km/h; Wind Direction = 242^0). The time (in minutes) the fire would take to reach each pixel is indicated by the colour of the pixel and by the number given next to points of interest (red points). The burned area extent mapped from Sentinel-2 imagery is overlaid in yellow. 43

Figure 28a. Oblique view of north-westerly wind flow and wind eddies forming in the valley on the lee side of the hill at 200 m altitude. 44

Figure 28b. Overhead view of north-westerly wind flow and wind eddies forming in the valley on the lee side of the hill at 200 m altitude. 45

Figure 29. Burn scar mapped from WorldView-3 imagery of 19 June 2017 (yellow outline), showing examples of V-shaped point ignitions probably related to "spotting" by the fire (white circles). 46

Figure 30. Burned area of the Elandskraal (west) and Kruisfontein (east) fires around Knysna displayed as a yellow outline on the Sentinel-2 images of 14 June 2017. The burned area is visible in shades of pink and remaining vegetation in shades of green. 47

EXECUTIVE SUMMARY

In the early hours of 7 June 2017, a set of circumstances triggered a number of disastrous wildfires in the Sedgefield-Knysna-Plettenberg Bay area that resulted in the deaths of seven people and the evacuation of over 10 000 residents. Damage to properties and infrastructure is estimated to amount to several billion Rand and large areas of commercial plantations were destroyed. It is arguably the worst fire disaster in South African history.

The Council for Scientific and Industrial Research (CSIR) responded by facilitating the activation of the *International Charter for Space and Major Disasters,* thereby gaining access to satellite data to assist in the response to the disaster. The CSIR, through the Advanced Fire Information System (AFIS) programme, was responsible for the acquisition, processing and production of value-added products from 500 gigabytes of satellite data that was made available through the charter in support of the Western Cape Disaster Management Centre (WCDMC). AFIS has been developed over the past 13 years to assist fire managers with the prediction, detection, monitoring and assessment of wildfires through a range of technologies and information services. The AFIS team's unique skills in the processing and production of geospatial fire products, enabled them to do a chronological, geospatial analysis of the Elandskraal fire. While there were two distinct fires in the Knysna area which both started on 7 June 2017, this report focuses only on investigating the origin and initial spread of the Elandskraal fire, as the cause and timing of the Kruisfontein fire are well-known. The cause, location and timing of the ignition of the Elandskraal fire was a contentious issue from the outset as limited data were available at the time. However, as more satellite and other data sets became available and were integrated, a probable sequence of events emerged. The assessment relied solely on the analysis of data that were captured before, during and after the fire, including images from various satellites, drone video footage, lightning and weather data, as well as a Bushnell motion-sensing camera that was positioned in the path of the fire. It is rare for the initial stages of a fire to have been documented so extensively by multiple sensors and instruments. Unfortunately, extensive cloud cover during the remainder of 7 June 2017 prevented analysing the progression of the fire towards Knysna. The report did not take other reports on the Elandskraal fire into consideration in order to provide an independent assessment.

The objective of this report was to use all relevant sensor data to provide a comprehensive, scientific analysis and interpretation of the sequence of events that led to the Elandskraal fire. To this end, the report analysed all available geospatial data sets to gain a better understanding of how, where and when this fire started and how it spread during the first 45 minutes. The report is directed at fire managers and AFIS stakeholders, specifically Western Cape Disaster Management Centre (WCDMC), Southern Cape Fire Protection Association (SCFPA), Department of Environmental Affairs (Chief Directorate: Natural Resource Management) and Department of Agriculture Forestry and Fisheries (Directorate: Forestry Regulations and Oversight). The document furthermore addresses the obligation towards the *International Charter for Space and Major Disasters* to report on how the satellite data were used to assess the disaster. The analyses provide valuable insight into conditions leading to this disastrous fire which may assist in mitigating fire risks and inform responses in future.

The sequence of events is summarised below:

Before the fire:

The southern and western Cape have been experiencing drought conditions since 2015 and long-term satellite image analyses indicates that the "Very dry scrub forest" in the Elandskraal area was very dry in months leading up to the fire.

A positive lightning strike was detected on 22 March 2017 (20h55) by the South African Weather Service (SAWS) South African Lightning Detection Network (SALDN) within the Elandskraal area. The exact location of a lightning strike is difficult to determine and is represented by an ellipse encompassing an extended area within which the strike may have been located anywhere with a 99% confidence.

On 29 March 2017, an area of decreased vegetation greenness of approximately 122 m² is first detected with the satellite imagery (Sentinel-2) in the north-western corner of Elandskraal. By 18 May 2017, the affected area has grown to approximately 3 033 m² in the Sentinel-2 satellite image.

Elandskraal residents commission a drone survey to search for the origin of smoke continuously rising from the valley on 27 May 2017. Drone video footage capture images of smouldering vegetation (33.9576 S 22.8398 E), within the 99% confidence ellipse of the lightning strike of 22 March 2017 and within the area of decreased vegetation greenness detected by Sentinel-2.

The start of the fire – 7 June 2017

A private weather station at Kooigoed, in the path of the fire, recorded weather conditions every 5 minutes. Between 1h03 and 1h30 berg wind conditions start intensifying with a sudden shift in wind direction from southerly to westerly winds at around 01h09. Average wind speeds increase from 5 km/h to 20 km/h with wind gusts of more than 30 km/h. Air temperature increasing from 19°C to 25°C and relative humidity decreased from 53% to 29%. Between 03h00 and 03h30 north-westerly winds reduced the relative humidity to 25% with gusts of up to 50 km/h by 03h30, 60 km/h at 05h10 and 55 km/h at 05h23.

It is estimated that the smouldering patch of vegetation (referred to as a "holdover" fire) flared-up between 05h00 and 05h30, based on Rothermel fire spread model simulations and the Meteosat Second Generation (MSG) satellite observation. A thermal anomaly indicating an active fire at Elandskraal is first recorded by the MSG satellite at 06h03 when the fire reached a minimum detectable size (0.4-0.6 ha per pixel at 700 Kelvin). The MSG detection of the Elandskraal fire may have taken up to 43 minutes based on the observations from the Kruisfontein fire on the time lag between the known ignition time and the corresponding first MSG detection. This suggests an estimated starting time for the Elandskraal fire of 05h20.

Initial spread of Fire:

A Bushnell motion-sensing camera at Kooigoed (33.9628 S, 22.855 E) first photographs the fire approaching from the north-west. The time that the fire took to spread from the 1-2 ha active fire detection with MSG (06h03) to Kooigoed (06h48) is estimated at 45 minutes. The distance between these two points is approximately 1 433 m, and thus the mean rate of spread was calculated at 31.8 m/min.

Damage to the croquet lawn and homestead (located 524 m south-east from the holdover fire) indicates a fire that approached from the north-west, burning and scorching the kikuyu lawn mostly on the north, north-eastern and north-western edges.

A Sentinel-2 image of 14 June 2017 was used to map the total burned area of the Elandskraal and Kruisfontein fires and the estimated area burned was 9 440 ha.

Conclusion

Based on the location and size of the holdover fire in relation to the final burn scar, the prevailing north-westerly berg wind conditions, as well as the direction from which the head fire propagated and burned into the croquet lawn and homestead, we conclude that the smouldering patch of vegetation observed in the drone footage on the 27 May 2017 and the Sentinel-2 imagery was the most probable cause of the Elandskraal fire.

Recommendations

Holdover fires have the potential to flare-up under severe weather conditions with potentially devastating consequences, as was seen in the Knysna fire disaster. In order to reduce the risks of these events in future, the AFIS team recommends the development of a Lightning-Induced Fire Ignition Probability Index for South African conditions. The introduction of such a probability index will allow for the early detection and alerting of positive lightning strikes specifically in areas with very dry vegetation fuels and the subsequent detection of patches of smouldering vegetation.

Fire risk along the wildland-urban interface (WUI) of the fynbos biome can be calculated and mapped using the geospatial assessment procedure (or framework) previously demonstrated by the CSIR for specific study areas (Forsyth and Le Maitre 2015). We recommend that the risk assessment procedure be expanded to the entire fynbos biome (or all fire-prone biomes in the country) and augmented by including data of fuel type, fuel load (biomass), fuel moisture and burn history (time since last burn), all of which can already be derived from satellite imagery on an ongoing basis. The local landowners and government should be very well informed about fire risk along the WUI and share the responsibility for mitigating the risk of wildfires (Forsyth and Le Maitre 2015). To this end, fire risks should be continuously assessed, with risk maps being publicly accessible through web-based geographic information systems. Earth Observation and geospatial technologies are sufficiently mature to provide essential fire risk and other fire related information demonstrated in this report, however sufficient funding is required to take this technology beyond the "proof-of-concept" or "pilot" phases towards an operational service. The mitigation of the risk of inevitable wildfires in the fynbos biome, will therefore require (i) more research on the occurrence and behaviour of lightning-induced holdover fires, (ii) the development of a system to map the Lightning-Induced Fire Ignition Probability Index based on lightning strike data and satellite data, (iii) a system for mapping fire risk in WUI and for publicly disseminating these maps, (iv) broader communication of fire danger based on weather conditions, (v) sufficient support and funding to maintain these operational, public-good, fire information systems and finally, (vi) close collaboration between local landowners and government by means of fire protection associations to mitigate fire risk.

1 INTRODUCTION

Previous reports by CSIR have highlighted the risks of fire to communities (economic assets and human life) in the wildland-urban interface (WUI), where urban development borders flammable vegetation of the fire-prone fynbos biome (Forsyth and Le Maitre 2015, Forsyth, Kruger and Le Maitre, 2010). The reports highlighted the increased likelihood of fire in relation to vegetation fuel type and fuel load along the WUI. As more people build homes in close proximity to natural vegetation, the WUI expands and the risk of wildfire increases. The wildfire risk in the fynbos biome of the western and southern Cape will remain high along the WUI and is exacerbated by extended droughts and extreme weather conditions, as was the case during the Knysna fires of 2017.

In the early hours of 7 June 2017, a set of circumstances triggered a series of disastrous wildfires in the Sedgefield-Knysna-Plettenberg Bay area that resulted in the deaths of seven people and the evacuation of over 10 000 residents. Over 1000 firefighting personnel from all over the country were deployed in an effort to bring the fire under control. Damage to properties and infrastructure is estimated to amount to several billion Rand and large areas of commercial plantations were destroyed. It is arguably the worst fire disaster in South African history. The extent and intensity of these fires is reminiscent of the 1869 “Great Fire” which raged out of control between Riversdale and Uitenhage for weeks, after a prolonged and severe drought and similar extreme fire danger conditions[1].

The two main fires that were reported on 7 June 2017 have been named the *Elandskraal Fire* and the *Kruisfontein Fire* respectively. The Elandskraal fire started 20 km north-west of the town of Knysna, while the Kruisfontein fire started 6 km to the east of Knysna. By 8 June 2017 the two fires had spread to Knysna and Plettenberg Bay, leaving a path of destruction in its wake and destroying more than 1000 houses.

The Council for Scientific and Industrial Research (CSIR) responded by facilitating and assisting in the activation of the *International Charter for Space and Major Disasters,* thereby gaining access to additional satellite data to assist in the response to the disaster. South Africa is not currently a member of the charter, but it allows for member countries to sponsor an activation for a non-member country with whom they cooperate in disaster management activities. The Provincial Disaster Management Centre (PDMC) of the Western Cape requested South Africa’s National Disaster Management Centre (NDMC) to formally request activation of the charter on 12 June 2017. The CSIR, through the Advanced Fire Information System (AFIS) programme, was responsible for the acquisition, processing and production of value-added products from 500 gigabytes of diverse satellite data that was made available through the charter in support of the Western Cape Disaster Management Centre (WCDMC). AFIS has been developed over the past 13 years to assist fire managers with the prediction, detection, monitoring and assessment of wildfires through a range of technologies and information services. The AFIS team’s unique skills in the processing and production of geospatial fire products, as well as the interpretation of fire events using diverse technology, enabled them to do an analysis of the Elandskraal fire (Figure 1).

[1] Website: https://www.georgeherald.com/News/Article/General/the-great-fire-of-1869-20170817, accessed: March 2018

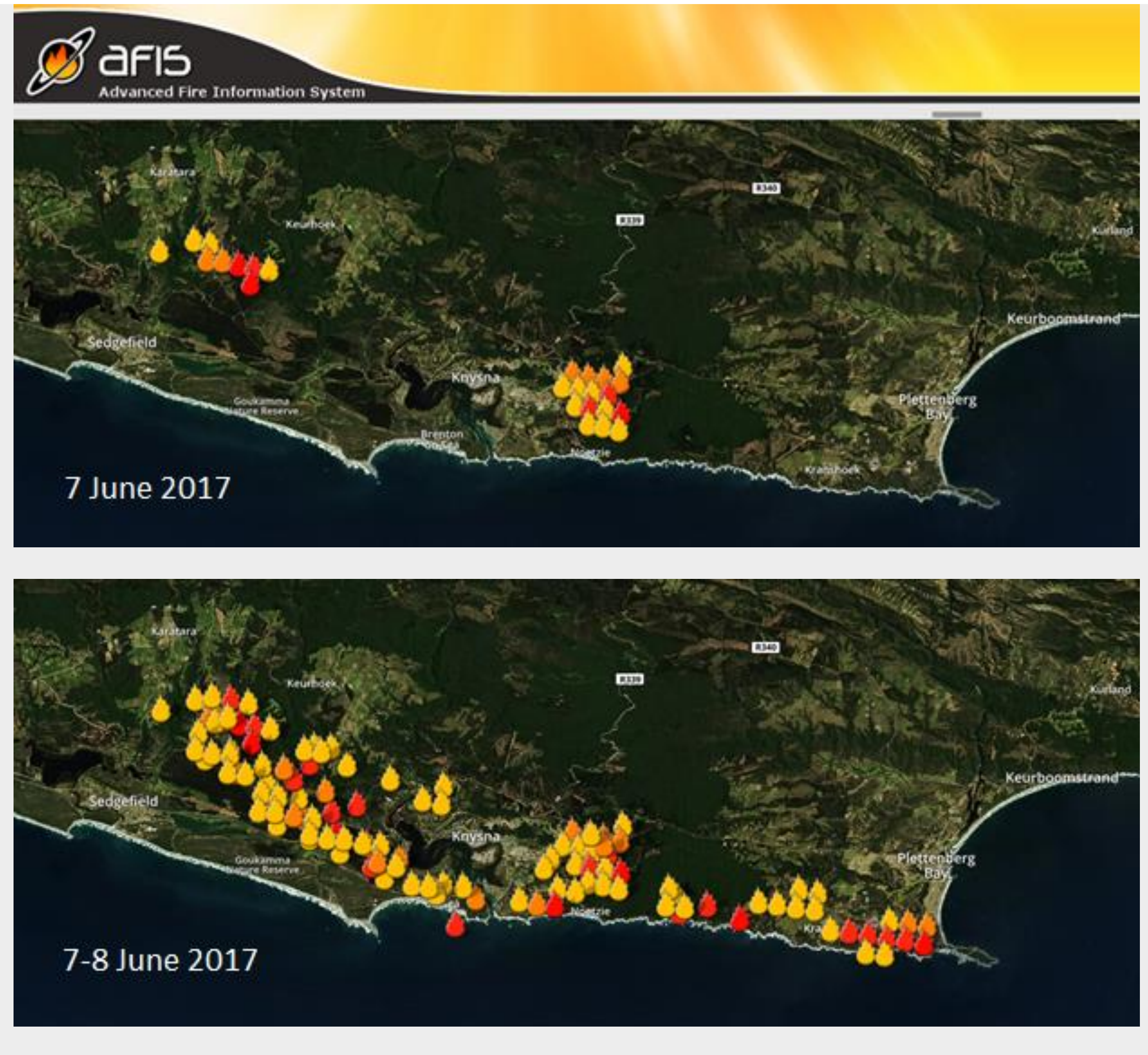

Figure 1. Active fires detected by MODIS and VIIRS satellite sensors on 7-8 June 2017 displayed in the online viewer of the Advanced Fire Information System (AFIS)[2].

Although there were two distinct fires in the Knysna area which both started on 7 June 2017, this report focuses only on investigating the origin and initial spread of the Elandskraal fire, as the cause and timing of the Kruisfontein fire are well documented. The cause, location and timing of the ignition of the Elandskraal fire was a contentious issue from the outset as limited data were available at the time. However, as more satellite and other data sets became available and were integrated, a probable sequence of events emerged. The assessment relied solely on the analysis of data that were captured before, during and after the fire, including images from various satellites, drone video footage, lightning and weather data, as well as a Bushnell motion-sensing camera that was positioned in the path of the fire. It is rare for the initial stages of a fire to have been documented so extensively by multiple sensors and instruments. Unfortunately, extensive cloud cover during the remainder of 7 June 2017 hampered analysis of the

[2] www.afis.co.za, accessed: March 2018

progression of the fire towards Knysna. The report thus focuses on the events leading up to the fire and analysis of the first hour of the fire in great detail. The report did not take other reports on the Elandskraal into consideration in order to provide an independent assessment.

The objective of this report was to use all relevant sensor data to provide a comprehensive, scientific analysis and interpretation of the sequence of events that led to the origin and initial spread of the Elandskraal fire. To this end, the report analysed all available geospatial data sets to gain a better understanding of how, where and when this fire started. The report is directed at fire managers and AFIS stakeholders, specifically the Southern Cape Fire Protection Association (SCFPA), Western Cape Disaster Management Centre (WCDMC), Department of Environmental Affairs (Chief Directorate: Natural Resource Management) and the Department of Agriculture Forestry and Fisheries (Directorate: Forestry Regulations and Oversight). The document furthermore addresses the obligation towards the International Charter for Space and Major Disasters to report on how the satellite data were used to assess the disaster. The analyses provide valuable insight into conditions leading to this disastrous fire which may assist in mitigating fire risks and inform responses in future.

The report is structured as follows:

- Study area
- Timeline of events
- Detailed technical analysis: Before the fire, Start of fire, Initial Spread of fire, After the fire
- Summary of technical analysis and conclusions
- Recommendations

2 STUDY AREA

The name Elandskraal refers to the original farm which has been subdivided into smaller land parcels. The Elandskraal farming area (hereafter referred to as "Elandskraal") is situated in the greater Knysna region (Figure 2a) which includes a 50 km stretch of the Garden Route from Sedgefield to Plettenberg Bay. The greater Knysna area encompassed the extent of the Elandskraal fire approximately 20 km north-west of the town of Knysna and the Kruisfontein fire 6 km to the east (Figure 2a). Further north of Knysna another large fire burned an extensive area near Uniondale during 6 and 7 June 2017. Figure 2b illustrates the full extent of the burned area of the Elandskraal and Kruisfontein fires in shades of pink amongst the green unburned vegetation in the Sentinel-2 satellite image (14 June 2017). The report mainly focused on a small portion of the Elandskraal area where the fire was believed to have started, in order to establish the ignition source and to analyse the initial spread of the fire to various points of interest (Figure 2c). The analyses were conducted at three nested scales; (i) the larger Knysna area (approximately 60 km X 50 km) (Figure 2a), (ii) the Elandskraal area (approximately 10 km X 10 km) (Figure 2b) and (iii) the probable origin of the fire in the north-western corner of Elandskraal burned area (approximately 2 km X 1 km) (Figure 2c).

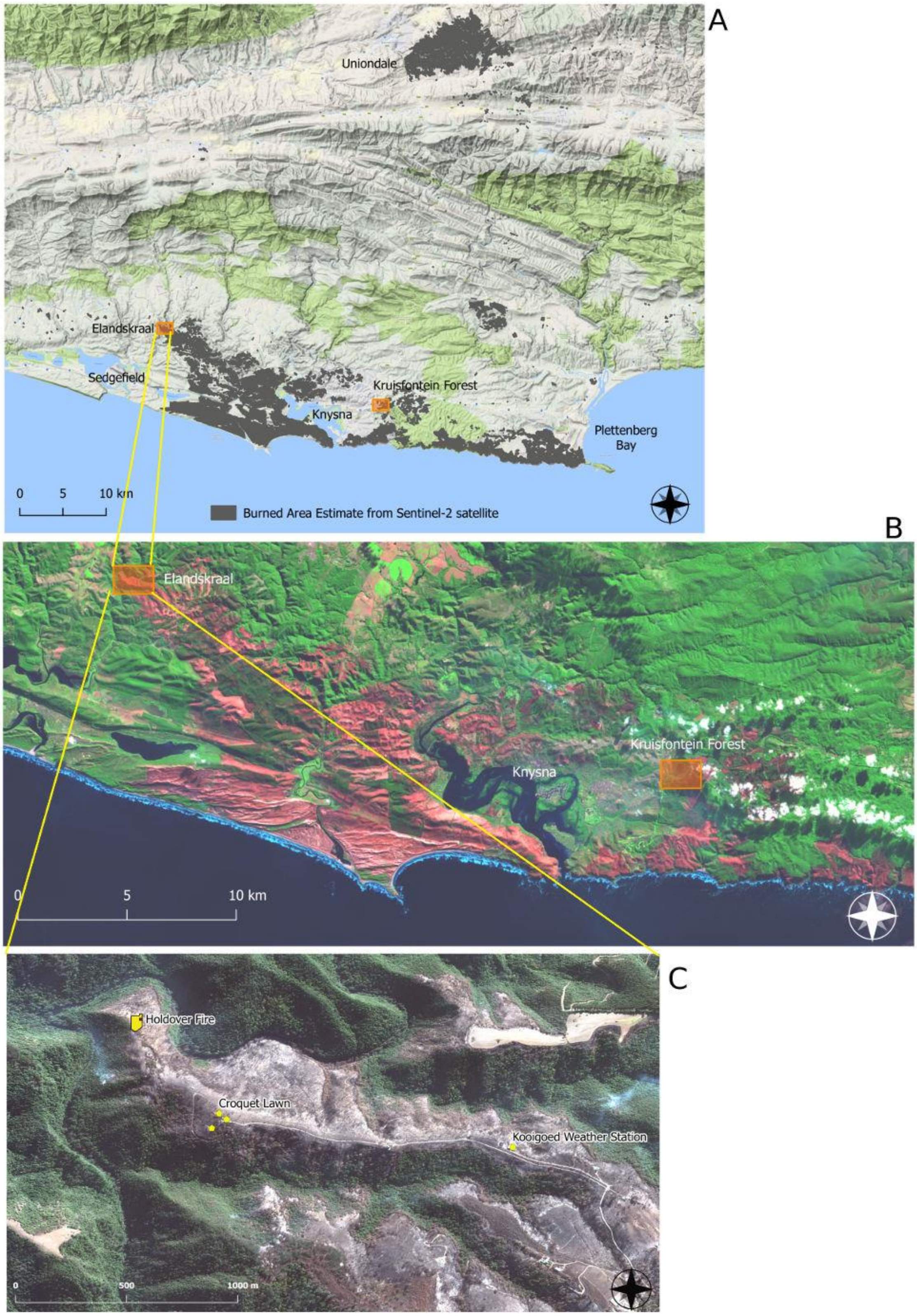

Figure 2. (A) Overview of the greater Knysna region of South Africa, indicating the burned area (dark grey) of the Uniondale, Elandskraal and Kruisfontein fires. (B) The burned area of the Elandskraal and Kruisfontein fires in shades of pink amongst the green unburned vegetation in the Sentinel-2 satellite image (14 June 2017). (C) WorldView-3 image (19 June 2017) of the probable origin of Elandskraal fire showing burned vegetation and the location of the "holdover" fire and the weather station at Kooigoed.

3 TIMELINE OF EVENTS

The following is a summary narrative of key events that occurred before (11 weeks prior up until Day -1), during (Day 0, 7 June 2018) and after (Day +1 to +12) the Elandskraal fire. The investigation of each event did not take place along the same timeline, but was pieced together in a retrospective manner.

<u>Before the Fire</u>

Months and weeks before: The southern and western Cape have been experiencing severe drought conditions since 2015. Analysis of long-term satellite time series (2002 to 2017) indicates a vegetation greenness and condition well below the long-term average by May 2017 and therefore vegetation was extremely dry and flammable. The vegetation in the Elandskraal area is described as “Very dry scrub forest”, and consists of a mixture of shrubs, trees and creepers.

19 March 2017: No sign of any vegetation anomalies in the satellite imagery (Sentinel-2) over the Elandskraal area.

22 March 2017: A positive lightning strike (20h55) was detected by the SAWS South African Lightning Detection Network (SALDN) within the Elandskraal area. The exact location of a lightning strike is difficult to determine and is represented by an ellipse encompassing an extended area within which the strike may be located with a 99% confidence.

29 March 2017: An anomaly in the vegetation identified as a reduction in relative greenness in a patch of approximately 122 m^2 is first detected with the satellite imagery (Sentinel-2) at 33.9576 S and 22.8398 E, in the north-western corner of the final Elandskraal burn scar. The vegetation anomaly detected in the Sentinel-2 satellite imagery is located within the 99% confidence ellipse of a positive lightning strike of 22 March 2017 detected at 18:55:54 GMT (20:55:54 SAST). Based on the intersection between the vegetation anomaly and the 99% confidence ellipse of the lightning strike of 22 March 2017, this particular lightning strike has the highest probability of all the strikes to have ignited the smouldering patch of vegetation.

20 April 2017: Vegetation anomaly is clearly discernible in a high resolution satellite image (GeoEye-1) in the north-western corner of the Elandskraal burn scar at 33.9576 S and 22.8398 E. The GeoEye-1 image is currently viewable in Google Earth and the patch of brown vegetation is clearly visible.

8 April, 5 May, 18 May 2017: Vegetation anomaly expanded to approximately 3 033 m^2 in satellite image (Sentinel-2).

27 May 2017: Elandskraal residents commission a drone survey to search for origin of smoke continuously rising from the valley. Drone video footage captures images of a patch of brown smouldering vegetation in the north-western corner of Elandskraal. Hereafter the smouldering patch is referred to as a “holdover fire”.

3-6 June 2017: Prefrontal weather conditions coupled with high winds prevailed, increasing the fire danger index to “severe” by 6 June. Berg wind conditions start to develop. The winds further dried and wilted the vegetation in the area that was already stressed due to severe drought.

Start of fire on 7 June 2017

01h03 to 03h48: MSG geostationary satellite detects no thermal anomalies as indications of active fires in Knysna area during continuous scans every 15 minutes.

01h08 and 01h10: The two polar orbiting satellite sensors (Aqua MODIS and NPP VIIRS) detect no thermal anomalies as indications of active fire anywhere in the Knysna area.

01h03 to 01h30: A weather station at Kooigoed (33.9628 S, 22.855 E), in the path of the fire, recorded weather conditions at 5 minutes intervals. Berg wind conditions start intensifying with a sudden shift in wind direction from southerly to westerly winds at around 01h09. Average wind speeds increase from 5 km/h to 20 km/h with wind gusts of more than 30 km/h. Air temperature increasing from 19°C to 25°C and relative humidity decreased from 53% to 29%.

03h00 to 03h30: Increase in wind speeds with north-westerly winds blowing downslope off the Outeniqua Mountains reducing the relative humidity further to only 25%. Wind gusts up to 50 km/h were recorded at 03h30.

03h30: A fire detected at Kruisfontein reported by a MTO Kruisfontein Plantation lookout tower.

04h03: MSG satellite detects an active fire at Kruisfontein, approximately 30 minutes after the start of the fire was observed and reported.

04h03 and 04h48: No evidence of any fires at Elandskraal by the MSG satellite

05h00 to 05h23: Wind gusts up to 60 km/h at 05h00 and 55 km/h at 05h23, when the weather station malfunctioned due to unknown causes.

05h00 to 05h30: Estimated time of **flare-up** of smouldering fire at Elandskraal based on time of first detection by MSG, Rothermel fire spread simulations and the subsequent time stamp observed by the Bushnell motion-sensing camera.

06h03: First evidence of a thermal anomaly indicating a fire at Elandskraal as detected by the MSG satellite when the fire reached minimum detectable size of 1-2 ha (within two MSG pixels).

Initial Fire Spread

06h48: Bushnell motion-sensing camera at Kooigoed (33.9628 S, 22.855 E) first photographs the fire approaching from the north-west. The time that the fire took to spread from the 1-2 ha active fire detection (06h03) to Kooigoed (06h48) is estimated at 45 minutes. The distance between these two points is approximately 1 433 m, and thus the mean rate of spread was calculated at 31.8 m/min.

After the Fire

12 June 2017: Activation of the *International Charter for Space and Major Disasters*.

The International Charter for Space and Major Disasters is an International Agreement between nations that allows for rapid access to high resolution satellite imagery from various space agencies and commercial satellite operators during and after a disaster. Upon activation, space agencies and commercial satellite operators task their satellites to capture imagery over the disaster area for two week period in support of relief efforts. The CSIR assisted the National Disaster Management Centre (NDMC) in the activation of the charter and directly supported the Western Cape Disaster Management Centre (WCDMC) and other fire agencies through the AFIS programme and by processing the satellite data made available by the charter.

14 June 2017: A Sentinel-2 satellite image of 14 June 2017 was used to map the total burned area of the Elandskraal and Kruisfontein fires and the first estimate of burned area is calculated at 9 440 ha excluding burned areas underneath forest canopies.

4 DETAILED TECHNICAL ANALYSIS

4.1 Sensors and Data

The datasets used for this investigation were captured before, during and after the fire and include satellite imagery, airborne drone video footage, active lightning strike detection, Bushnell motion-sensing camera photographs and weather station data. These data sources are briefly introduced below. The information was collected between 19 March and 14 June 2017 (Figure 3).

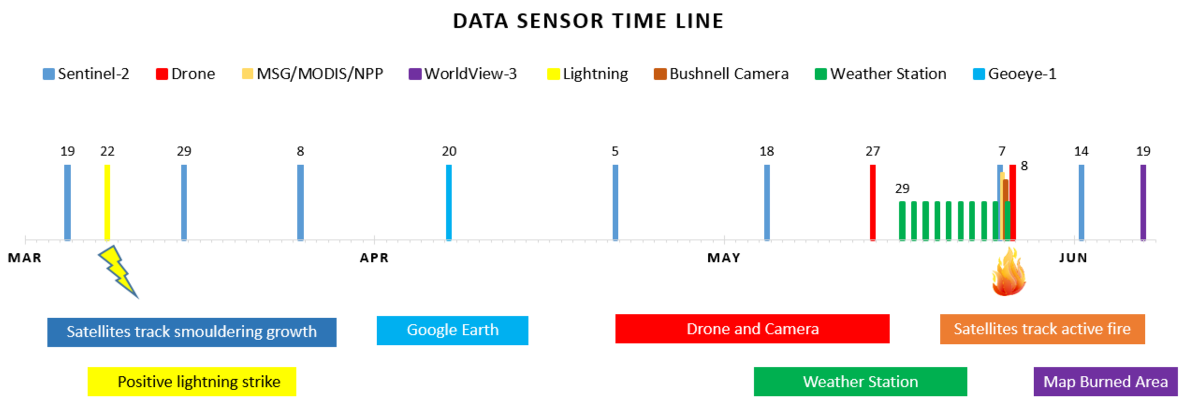

Figure 3. A timeline of diverse datasets used in the analysis of the Elandskraal fire from 19 March to 19 June 2017.

Sentinel-2 (10 m resolution) and WorldView-3 (30 cm resolution) satellites acquire images of the earth in the visible and near-infrared spectral range. Burned areas are routinely mapped using data from these satellites as they both have a short-wave infrared band (SWIR) used for mapping recently burned areas. Sentinel-2 is an Earth Observation satellite mission developed by the European Space Agency (ESA) as part of the Copernicus program to perform terrestrial observations in support of services such as forest monitoring, land cover change detection and natural disaster management. The Sentinel-2 satellite has been operational since 2016 and provides multi-spectral data with 13 bands in the visible, near infrared, and short-wave infrared part of the spectrum, revisiting a location every 10 days under the same viewing angles[3]. WorldView-3 is a commercial Earth observation satellite owned by DigitalGlobe. The spatial resolution is the highest level of detail commercially available from satellite imagery (30 cm).

Environmental satellites such as NOAA AVHRR and Terra and Aqua have been used for active fire detection for over 25 years. Fire detection is possible through radiant energy increases with temperature (Planck's law), producing a high contrast fire pixel relative to cool surrounding non-fire pixels (Matson and Dozier, 1981). Small increases in an object's temperature result in large increases in radiance in the mid-wave infrared (MWIR) (4 μm) and small increases in the long-wave infrared (LWIR) (11 μm) enabling sub-pixel size fire detection (Dozier, 1981; Matson & Dozier, 1981). Active fire detection algorithms either evaluate individual pixel values relative to a threshold (Flannigan & Vonder Haar, 1986); compare a pixel's temperature contextually to its neighbouring pixels (Flasse & Ceccato, 1996; Giglio *et al*., 2003); or track temporal changes in the MWIR (4 μm) brightness temperatures (Lasaponara *et al*., 2003).

The Moderate Resolution Imaging Spectroradiometer (MODIS) sensor is on both the Terra and Aqua satellites, and together with the National Polar-orbiting Partnership (NPP) Visible Infrared Imaging Radiometer Suite (VIIRS) sensor on the SUOMI satellite, detect active fires at 1 km and 375 m resolutions respectively. The MODIS sensors each have a 2 330 km wide viewing swath allowing the same area to be observed four times per day in 36 discrete spectral bands. The Terra MODIS sensor is in a descending, sun-synchronous orbit with observation times around 10h30 and 22h30, while the Aqua MODIS sensor is in an ascending orbit with observation times of 14h00 and 02h00[4]. The VIIRS sensor on board the SUOMI NPP satellite has a 3 000 km wide viewing swath enabling full earth coverage on a daily basis with a local overpass time of around 14h30 and 02h30 in 22 spectral bands including a new 375 m MWIR band enabling improved fire detection compared to the MODIS sensor[5] .

The Meteosat Second Generation (MSG) geostationary satellites carry the Scanning Enhanced Visible and InfraRed Imager (SEVIRI). SEVIRI measures 12 spectral channels that are optimized for the measurement of meteorological parameters. An active fire signal is represented by an increment of the radiance around the 4 μm wavelength with respect to the surrounding area. A complete scan of the Earth takes place every 15 minutes consisting of a 12-minute scan (8 segments) and a 3-minute calibration before the next scan. The Southern Cape is covered by the 2nd segment scan that is completed within 3 minutes of the 12-minute full disk scan with a pixel size of approximately 3.6 km x 3.6 km.

Due to the sensor characteristics of MSG, fires at southern latitudes can only be detected once they reach a minimum size and temperature, based on the minimum detectable fire size (Figure 4) (Calle *et al.* 2006; Laneve *et al.* 2006). The theoretical analysis of the minimum detectable size, including atmospheric effects and saturation conditions are especially important to delimit the operational range of this sensor in Southern Cape latitudes. During the evening, fires are more easily detected due to a cooler background surface temperature. Assuming a forest fire temperature of 700K, a single MSG pixel could detect a fire of between 0.4 ha to 0.6 ha at southern latitudes (Figure 4).

---

3 https://sentinel.esa.int/web/sentinel/missions/sentinel-2, accessed: March 2018
4 https://terra.nasa.gov/about/terra-instruments/modis, accessed: March 2018
5 https://www.nasa.gov/pdf/596329main_NPP_Brochure_ForWeb.pdf, accessed: March 2018

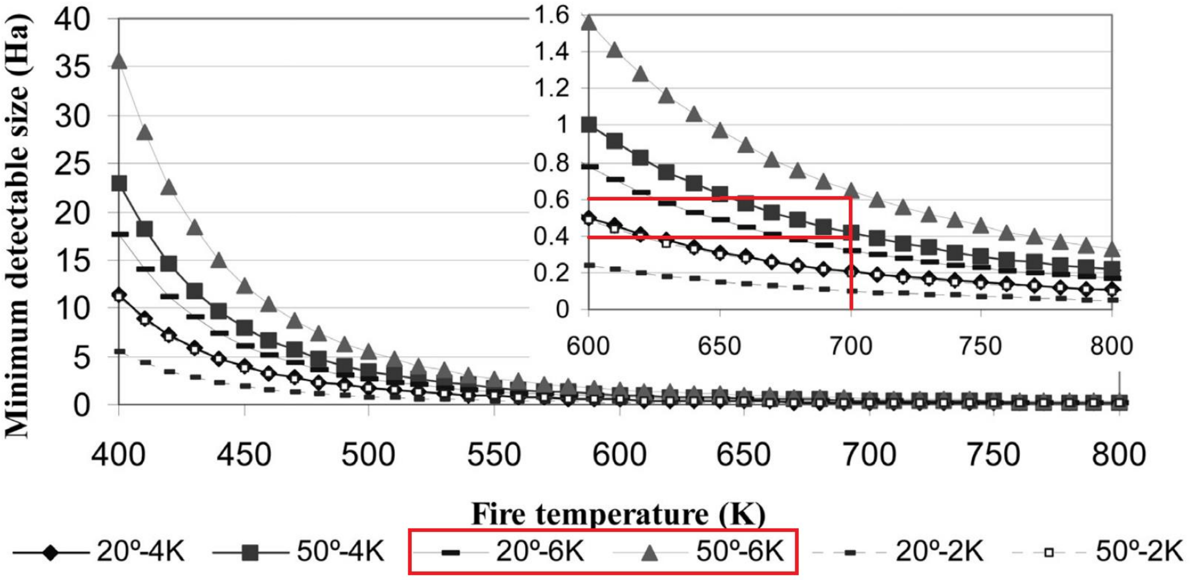

Figure 4. Minimum size of fire (ha) that can be detected by SEVIRI sensor on MSG satellite, at different fire temperatures and latitudes, taking atmospheric attenuation into account (from Calle *et al*. 2006). For the Elandskraal latitude of 34°, the range between 20° and 50° latitude where used where the thermal gradient of 6K/15 minutes is applicable to night time atmospheric attenuation.

A summary of dates and times when data were captured by the sensors used in the investigation are provided in Table 1.

Table 1/...

Table 1. List of sensors used in analyses along with their sources and details of date and time of acquisition. (details of sensors are available by following the provided hyperlinks)

SENSOR	***DATE***	***TIME***
Sentinel-2 satellite (Copernicus, ESA)	*19 March 2017*	*10h38*
	29 March 2017	*10h34*
	8 April 2017	*10h37*
	5 & 18 May 2017	*10h37*
	7 June 2017	*10h39*
	14 June 2017	*10h28*
WorldView-3 satellite (DigitalGlobe: Charter Call 615)	*19 June 2017*	*11h17*
MSG SEVIRI infrared satellite (EUMETSAT)	*7 June 2017*	*01h03-15h48*
MODIS Terra satellite (NASA, USGS)	*7 June 2017*	*10h26*
	8 June 2017	*11h10*
MODIS Aqua satellite (NASA, USGS)	*7 June 2017*	*01h08*
	7 June 2017	*14h46*
	8 June 2017	*13h51*
NPP VIIRS satellite (NOAA)	*7 June 2017*	*01h10*
	7 June 2017	*13h28*
	8 June 2017	*14h49*
Google Earth: GeoEye-1 satellite (DigitalGlobe)	*20 April 2017*	*unknown*
Aerial drone footage (Elandskraal community)	*27 May 2017*	*unknown*
	8 June 2017	*unknown*
Private Weather Station Kooigoed (Vital Fire)	*29 May – 7 June 2017*	*5-minute intervals*
Vaisala lightning detections (SALDN, SAWS)	*22 March 2017*	*20h55*
Bushnell Wireless Trophy Cam HD (motion-sensing camera) (Elandskraal community)	*7 June 2017*	*06h48-9h15*

4.2 Before the fire

4.2.1 Drought and vegetation condition

The southern and western Cape have suffered drought conditions since 2015. The Knysna municipality has had water concerns since March 2016[6] and implemented Level 3 water restrictions on 20 March 2017[7]. Due to low rainfall and subsequent reduced river flow, the surface level of the Garden Route Dam near George has been "low" and "very low" since March 2016 (Figure 5).

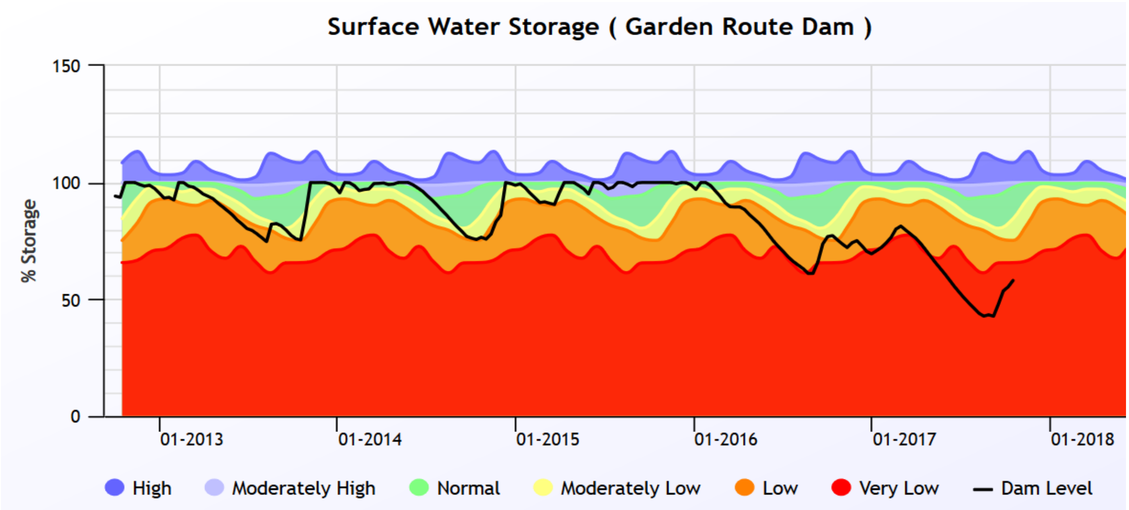

Figure 5: Garden Route Dam level from 2014 to 2017: National Integrated Water Information System (NIWIS)[8].

The impact of the drought on the vegetation photosynthetic activity in the Elandskraal area was investigated with a time-series of MODIS Enhanced Vegetation Index (EVI) satellite data. Satellite sensors can quantify what fraction of the photosynthetically active radiation is absorbed thereby characterising the health of the vegetation through a simple index (Tucker, 1979, 1996, Holben, 1986 and Gallo, 1990).

The Enhanced Vegetation Index (EVI) (Liu and Huete, 1995) is an optimised vegetation index designed to enhance the vegetation signal with improved sensitivity in high biomass regions, such as the Southern Cape. The EVI is more responsive to canopy structural variations than standard vegetation indexes such as NDVI, including leaf area index (LAI), canopy type, plant physiognomy and canopy architecture (Jiang *et al*, 2008), and is therefore well equipped to identify anomalies in vegetation condition. The typical EVI values are between -1 and 1 where low EVI between 0 and 0.2 indicate no photosynthetic activity typical of bare soil or stressed vegetation, and high EVI values above 0.6 indicate full canopy cover of very green forest canopy (Huete *et al.,* 2002).

The long-term average EVI was calculated for the area from 2002 to 2017 as historical reference and is shown in Figure 6 as the red line. The average EVI values for 2016 are plotted as a reference of the vegetation growth in the previous year to the fire. The EVI values for 2017 were plotted up to September.

[6] Source: https://www.businesslive.co.za/bd/national/2016-03-10-ongoing-drought-feeds-fears-knysna-taps-may-dry-up/, accessed: March 2018
[7] Source: http://www.knysna.gov.za/news/level-3-water-restrictions-implemented/, accessed: March 2018
[8] Source: http://niwis.dws.gov.za/niwis2/SurfaceWaterStorage, accessed: March 2018

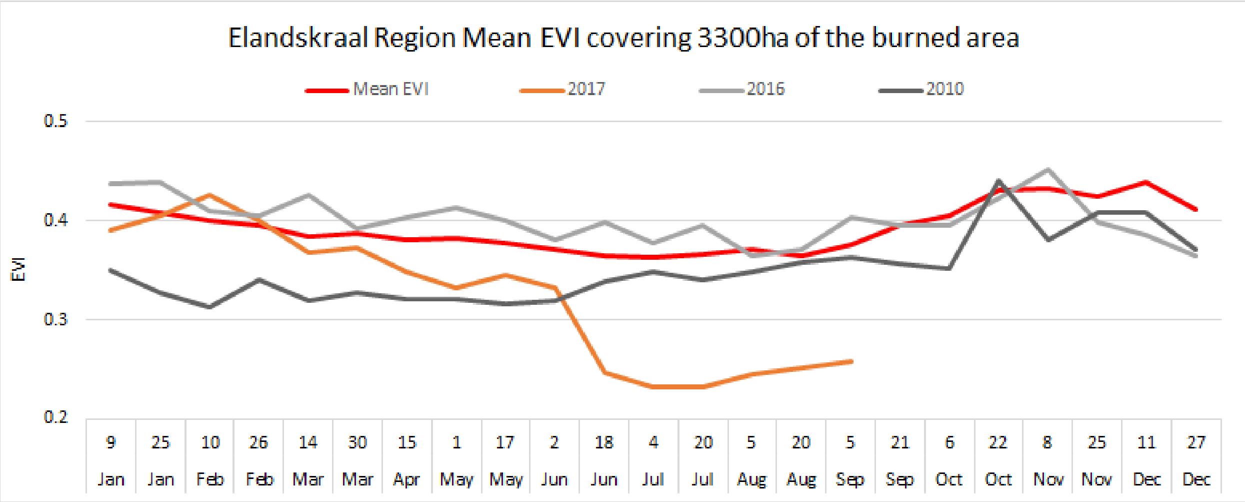

Figure 6: The long-term mean EVI (red) compared to 2016 (light grey) and 2017 (brown) of the 3 300 ha burned area in the Elandskraal. The EVI of 2010 provides a reference for very dry conditions (dark grey).

A consistent decrease in the EVI can be observed from March to June of 2017 with vegetation condition at well below the long-term average on 1 May 2017. Figure 6 also includes the EVI for the year 2010 as a reference, since it was a very dry year with the lowest EVI values in this area. It is evident that the EVI of 2017 was systematically decreasing towards that of 2010 between March and June 2017. This indicates that the vegetation was under stress attributed to the low rainfall. The sharp drop in EVI below 0.3 between 2 and 18 June can be attributed to the burned vegetation following the Elandskraal fire on the 7 June. The satellite-derived EVI data confirms that drought conditions prevailed on 7 June 2017, which contributed to the severity of the fire.

4.2.2 Vegetation type

The vegetation type where the holdover fire was identified falls within the Southern Cape Afrotemperate Forests[9] and is dominated by Dry or Scrub Woodland Forest (Geldenhuys, 1982). Scrub woodland is an indigenous forest type which is a transition between fynbos and thicket or forest and has developed as a successional stage from fynbos in the absence of fire. The natural, original untransformed vegetation units of the Elandskraal area form a mosaic of forest patches described as the Groot Brak River and Floodplain in the riverine areas, the Wilderness Fynbos-Forest on the slopes (scrub woodland) and the Hoogekraal Sandplain Fynbos on the crests (Vlok *et al.,* 2008). However, due to the absence of fire, the fynbos on the crest has transitioned to scrub woodland. These plant communities have been invaded by alien vegetation, including the surrounding riverine vegetation, and pose a serious fire hazard.

Very dry scrub forest, as described by von Breitenbach (1974), occurs on sites with a hot dry climate and sandy, loam or clay soils that dry out rapidly. The vegetation consists of a mixture of shrubs, trees and creepers that form an impenetrable, tangled woodland. Von Breitenbach (1974) observed that the very dry scrub forest and woodland floor is covered with dry leaf litter. The dry leaf litter expected in drought-affected forests would be the perfect fuel to support smouldering in a holdover fire. Burned area statistics calculated from MODIS satellite sensors from 2000 to present, show that the area under investigation has

[9] South African National Biodiversity Institute. 2012 Vegetation Map of South Africa, Lesotho and Swaziland [vector geospatial dataset] 2012. Available from the Biodiversity GIS website, downloaded on 18 October 2017

not had a significant fire since 2002 and was therefore at high risk of a severe fire based on the accumulated fuel load.

4.2.3 Smouldering vegetation

On 27 May 2017, residents of the Elandskraal community commissioned a drone survey to record video footage to determine the source and exact location of a smoke plume that was visible in the Elandskraal valley.

Figure 7: Drone footage taken on 27 May 2017 showing a smouldering patch of brown vegetation in the north-west corner of Elandskraal along the Karatara River (33.957624 S, 22.839807 E).

The existence of drone footage (Figure 7) showing a smouldering patch of vegetation was first brought to the attention of the CSIR by the Knysna Municipality in August 2017. The CSIR subsequently acquired the original, unedited video footage of both 27 May 2017 and 8 June 2017 from the Elandskraal community for further analysis in order to determine the location and possible cause of the smouldering vegetation. The drone footage was geolocated through a visual analysis of terrain features such as topography, the position of the Karatara River, unique features such as individual trees and roads which were co-located on both the drone imagery and a high resolution GeoEye-1 satellite image of 20 April 2017, publicly available on Google Earth (Figure 8). The GeoEye-1 image confirmed both the location of the drone footage and the existence of a patch of brown, potentially dying vegetation on a north-facing slope at Latitude: 33.957624 S, Longitude: 22.839807 E. The drone footage of 27 May 2017 identified the existence of a smouldering patch of vegetation eleven days before the fire on 7 June 2017.

Figure 8: Visible evidence of brown vegetation in the GeoEye-1 satellite image of 20 April 2017 displayed in Google Earth (33.957624 S, 22.839807 E).

Knowledge of the existence and location of the smouldering patch of vegetation allowed for a time-series analysis of historical satellite data to determine the date when satellites first identified an anomaly in the vegetation. Satellite imagery was also analysed to calculate the rate at which the smouldering patch of vegetation was growing. Satellite time-series data are routinely used to analyse fire disturbances in forests through the identification of spatial and temporal variations in vegetation condition (Goetz *et al*., 2006 and Bajocco *et al*., 2015).

Sentinel-2 Enhanced Vegetation Index (EVI) data are produced every 10 days as part of the AFIS Burned Area program and was analysed for the period from January 2017 to June 2017 to identify any vegetation anomalies (decrease in relative greenness) within the Elandskraal area. Sentinel-2 data were first processed to surface reflectance by applying an atmospheric correction (Sen2Cor[10]) before calculating the EVI's.

The Sentinel-2 satellite captured the first evidence of an anomaly in the EVI on 29 March 2017 (Figure 9b). The EVI values for the image of 19 March 2017 did not show any evidence of a decrease in vegetation greenness (Figure 9a). The patch of lower EVI values grew in size over time as shown by the series of cloud free images from 29 March to 18 May (Figure 9b-e). The area of the smouldering vegetation (Figure 7) was defined using a threshold to identify affected vegetation based on an EVI value of less than 0.5 and an EVI difference greater than 12% between 19 March 2017 imagery (before the affected area was detected) and

[10] http://step.esa.int/main/third-party-plugins-2/sen2cor/, accessed: March 2018

each of the images in the time series from March to May. The image of 18 May 2017 was the last cloud-free Sentinel-2 acquisition before the fire of 7 June 2017.

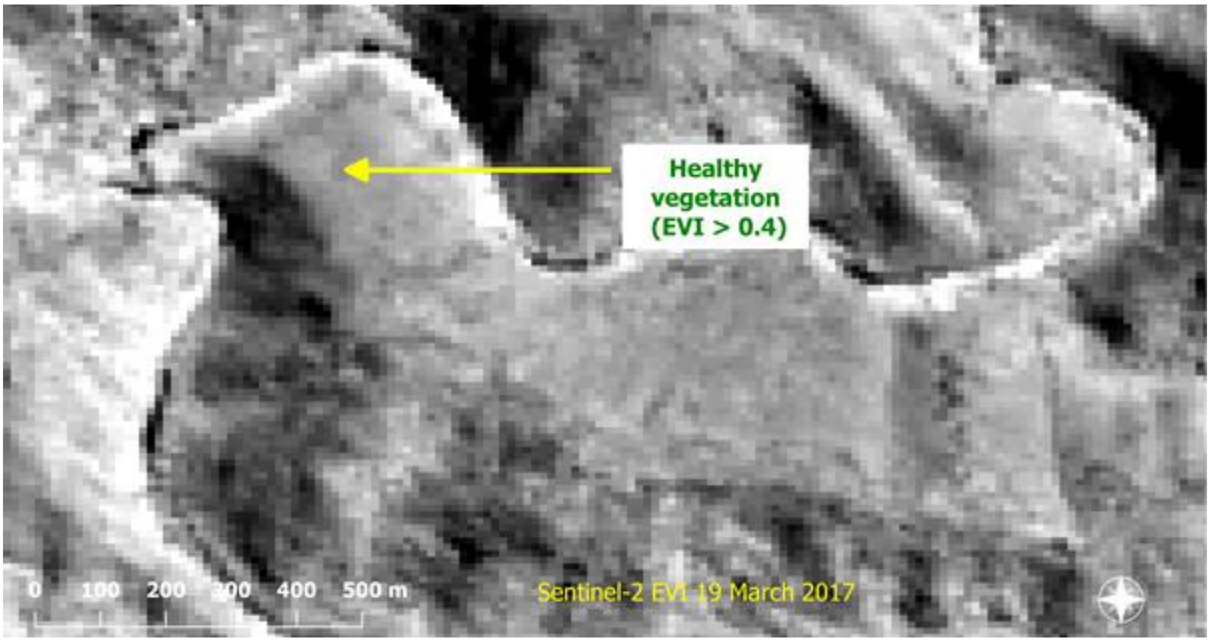

Figure 9a: Enhanced Vegetation Index (EVI) of Sentinel-2 imagery of 19 March 2017. The vegetation at the location of the subsequently identified smouldering patch has EVI values greater than 0.4 which is an indicator of healthy vegetation.

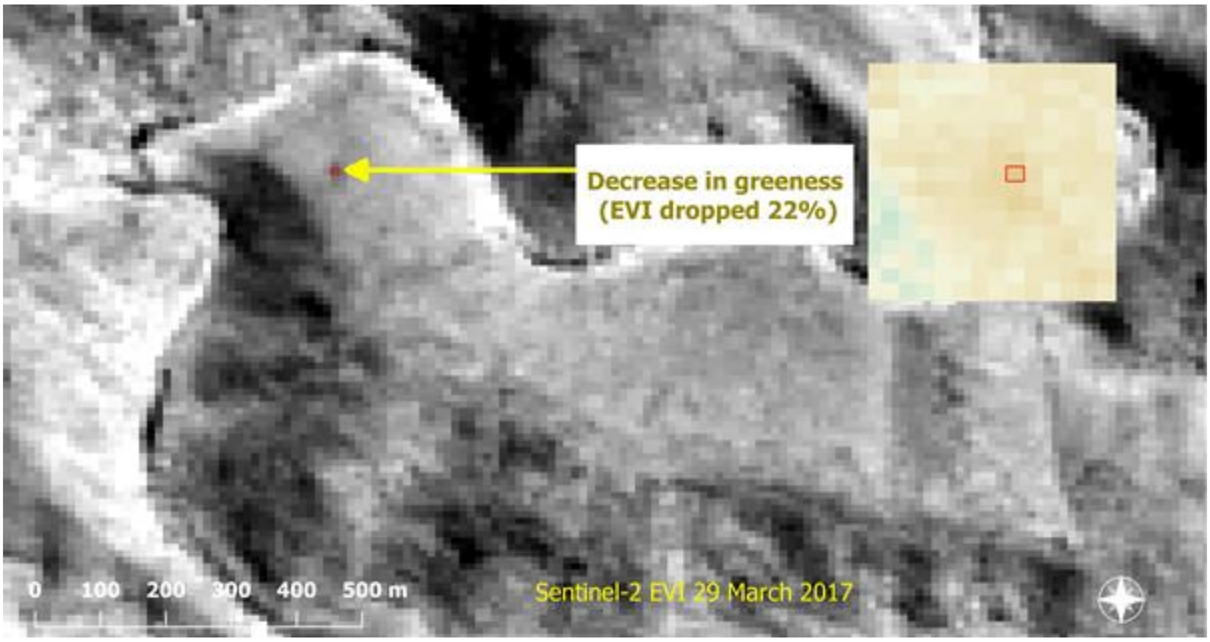

Figure 9b: Enhanced Vegetation Index (EVI) of Sentinel-2 imagery of 29 March 2017. EVI values have decreased from 0.41 to 0.32. A decrease in greenness is an indicator of vegetation stress as depicted in the inset map, where brown = decrease and green = increase in vegetation greenness between the 19 and 29 March 2017.

The inset map in Figure 9b shows the difference in EVI where brown indicates a decrease in greenness of the vegetation and green indicates the increase in greenness of the vegetation between the 19 and 29 March 2017 imagery. The EVI values within the vegetation anomaly decreased at a higher rate than the surrounding area. Between the 29 March and 8 April 2017 a decrease in EVI was noted (Figure 9c) and the size of the vegetation anomaly increased.

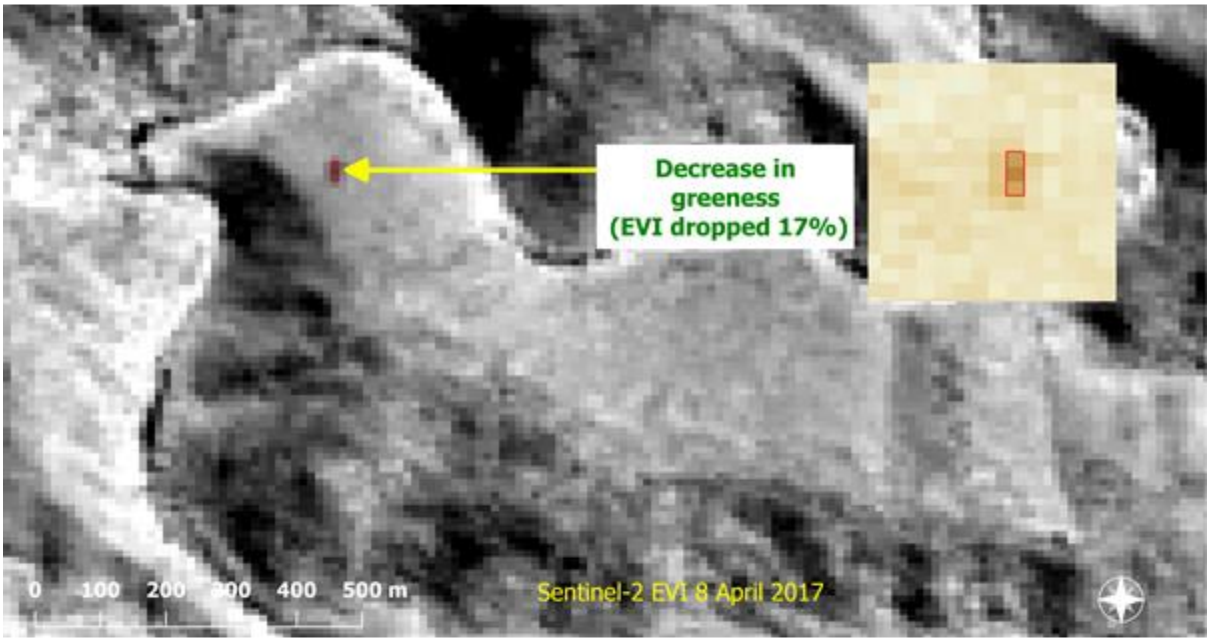

Figure 9c: Enhanced Vegetation Index (EVI) of Sentinel-2 imagery of 8 April 2017 where the pixel EVI values have decreased by 17% and the size of the vegetation anomaly has increased. A decrease in greenness is an indicator of vegetation stress as depicted in the inset map, where brown = decrease and green = increase in vegetation greenness between the 19 March and 8 April 2017.

Two cloud-free images were available in May and the expansion of the vegetation anomaly was measured using the changes in EVI values between dates and the number of pixels that contributed to the anomaly. On 5 May 2017 the EVI value decreased to 0.28 (Figure 9d) and by 18 May 2017 the decrease in EVI had stabilised at an EVI of 0.28 (Figure 9e). However, the size of the anomaly increased dramatically between the April and May measurements as illustrated in the inset maps in Figures 9d, 9e and Figure 10.

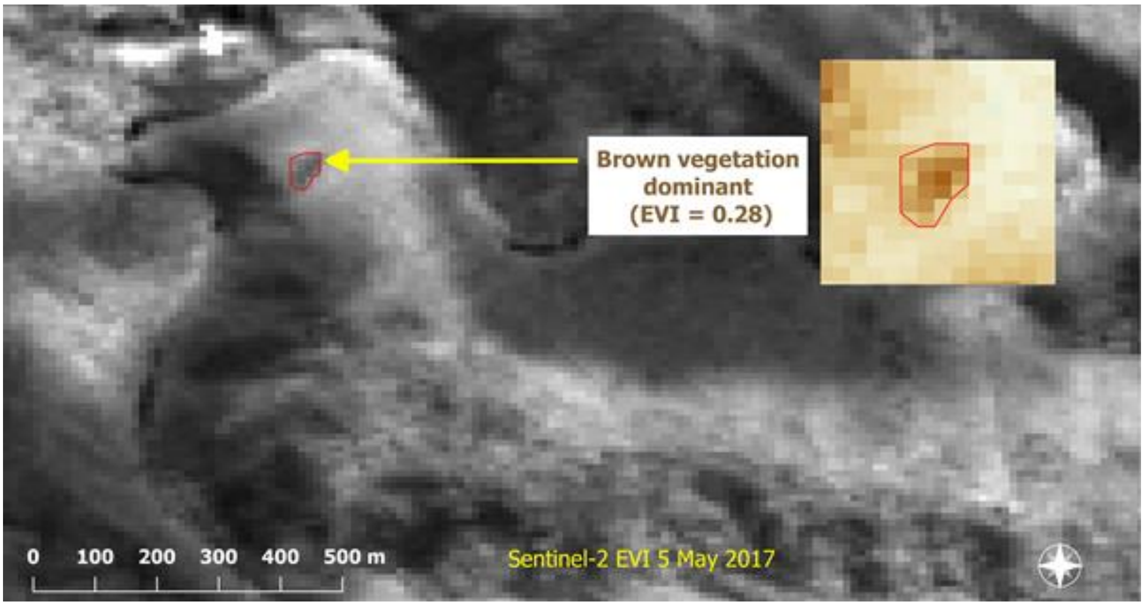

Figure 9d: Enhanced Vegetation Index (EVI) of Sentinel-2 imagery of 5 May 2017 where the pixel EVI values have dropped to 0.28 and the size of the anomaly has increased. A decrease in greenness is an indicator of vegetation stress as depicted in the inset map, where brown = decrease and green = increase in vegetation greenness between the 19 March and 5 May 2017.

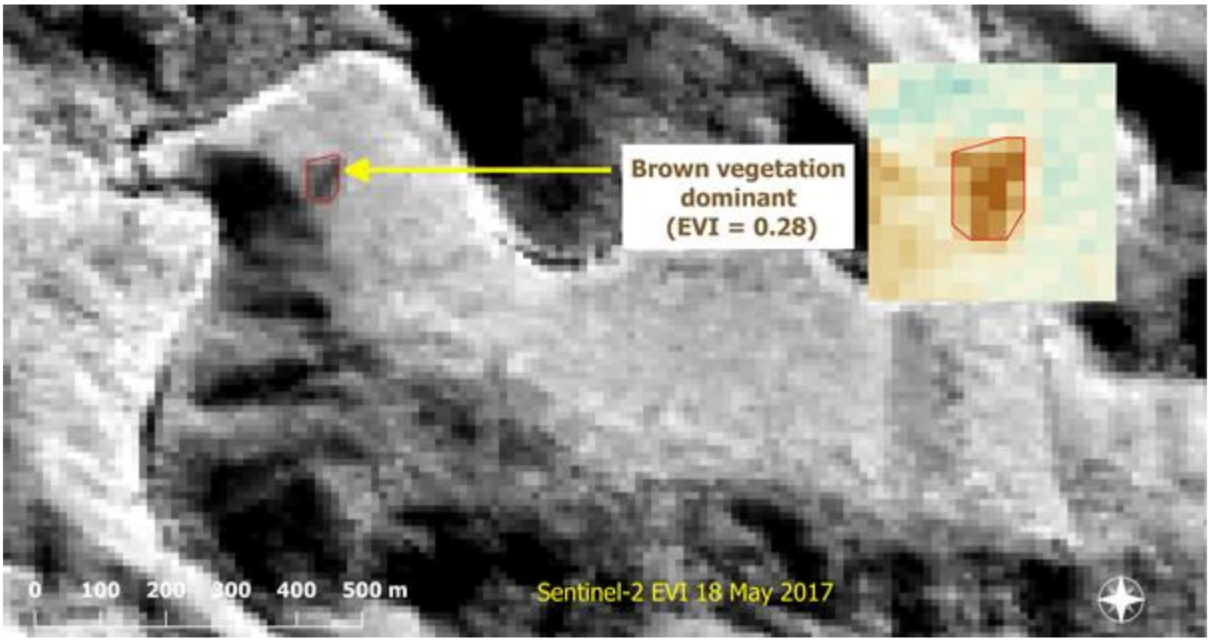

Figure 9e: Enhanced Vegetation Index (EVI) of Sentinel-2 imagery of 18 May 2017 where the pixel EVI values have stabilised at 0.28 but the size of the vegetation anomaly has increased to 3 033 m^2. A decrease in greenness is an indicator of vegetation stress as depicted in the inset map, where brown = decrease and green = increase in vegetation greenness between the 19 March and 18 May 2017.

The estimated area of affected vegetation increased from approximately 122 m^2 on 29 March 2017 to over 3 033 m^2 by 18 May 2017 (Figure 10). The average rate of expansion of the vegetation anomaly was calculated as approximately 50 m^2/day. The size of the vegetation anomaly was estimated to have grown to 3 488 m^2 by 27 May, which corresponds to the date of the drone footage, and to 3 994 m^2 (0.4 ha) by 6 June 2017, assuming an average rate of expansion of 50 m^2/day.

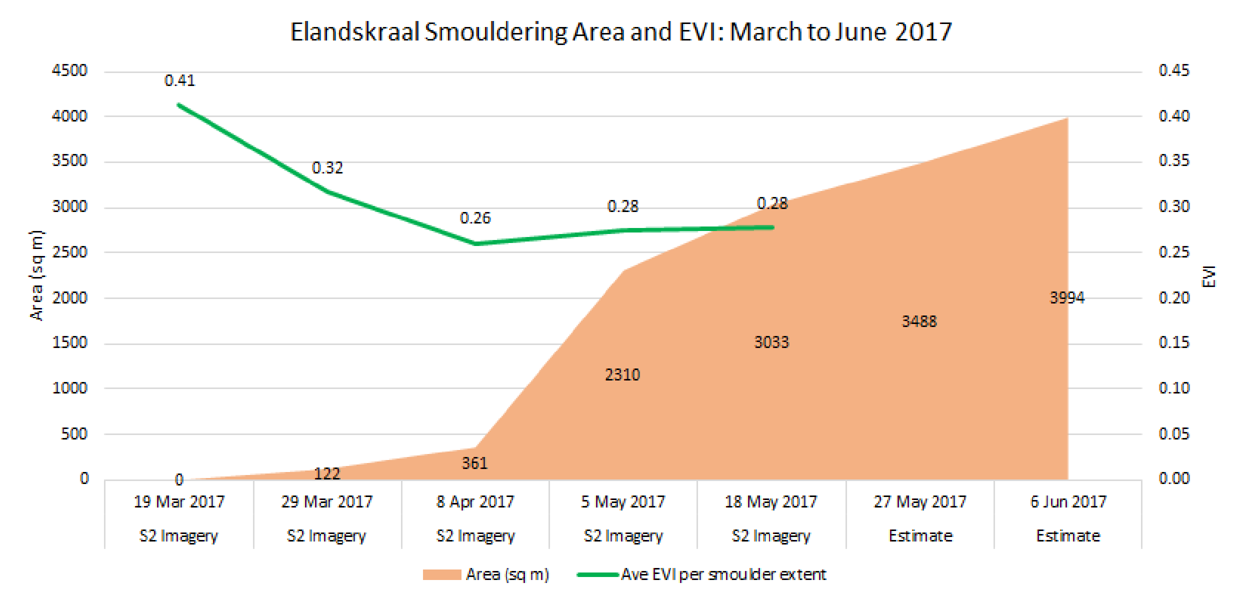

Figure 10. Area of vegetation affected by the smouldering fire at Elandskraal from 19 March to 18 May 2017, including the estimated area by 27 May and 6 June based on the average rate of growth of 50 m^2/day. The average Enhanced Vegetation Index (EVI) of all pixels within the growing smouldering area (green line).

The growth of the vegetation anomaly was mapped on the Sentinel-2 EVI imagery of 18 May to illustrate the expanding spatial extent of the affected area (Figure 11). The expansion of the anomaly is also displayed over the final Elandskraal burn scar recorded by the WorldView-3 satellite imagery captured on 19 June (Figure 12). The brown smouldering vegetation recorded in the drone footage on 27 May 2017 was therefore within the bounds of the Elandskraal burn scar with first evidence of affected vegetation by 29 March 2017. The estimated size of the resulting patch of stressed or dying vegetation potentially due to an underground smouldering fire was 3 994 m^2 by the morning of 7 June 2017. No sign of any other vegetation anomalies indicating a reduction in vegetation greenness could be identified elsewhere in the Elandskraal area.

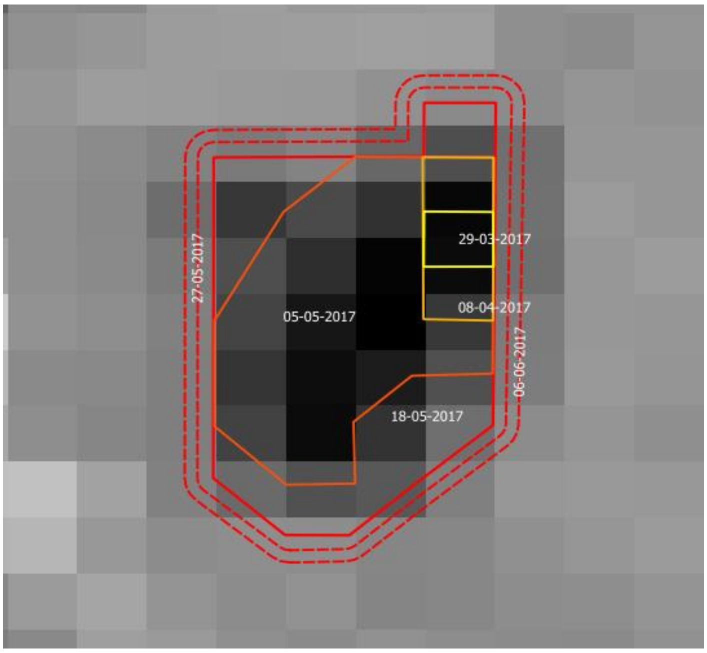

Figure 11: Spatial expansion of the smouldering patch of vegetation according to Sentinel-2 imagery and the estimate for the continued expansion between 27 May and 6 June based on the average rate of expansion. Background image is Sentinel-2 EVI of 18 May 2017.

Figure 12: The expansion of the vegetation anomaly (Figure 11) for different Sentinel-2 dates (green = 29/03/2017; pink = 8/4/2017; purple = 5/5/2017; olive green = 18/5/2017) with a background image of the WorldView-3 image of 19 June 2017 showing the Elandskraal burned area after the fire.

4.2.4 Lightning as a potential source of ignition

The Southern Cape Scrub woodland forests are tolerant of burning, and are considered to be fire-adapted vegetation, especially on the dry north-facing slopes (Geldenhuys, 1982). Because of the low humidity conditions and the existence of a prolonged drought, north-facing slopes would become more vulnerable to lightning-induced fires (Granger, 1984). Fires in the Southern Cape are predominantly caused by humans or through lightning strikes (le Roux, 1979). Both Edwards (1984) and le Roux (1979) reported lightning to be responsible for approximately 30% of the fires in the Southern Cape region. Despite having a relatively low incidence of lightning, data from Horne (1981) suggests that the southern parts of the Western Cape experience a far higher incidence of lightning-induced fires than elsewhere in South Africa.

Lightning was therefore investigated as a potential source of ignition based on the evidence of a vegetation anomaly (reduced vegetation greenness) identified by the Sentinel-2 EVI time series analysis that was confirmed to be smouldering vegetation by the drone video footage on 27 May 2017. In 2005, the South African Weather Services (SAWS) installed a state-of-the-art, cloud-to-ground lightning detection network developed by Vaisala. The South African Lightning Detection Network (SALDN) consists of 23 sensors across the country detecting electromagnetic signals emitted by lightning discharges (Gill, 2008).

Lightning strike information for 1 January 2017 to 7 June 2017 was obtained by CSIR from the South African Weather Services (SAWS) for an area of approximately 20 km X 20 km around Elandskraal (Figure 13). A total of 453 strikes were detected within the area of Elandskraal consisting, of 32 positive strikes (7% of strikes) and 421 negative strikes (93% of strikes) (Figure 13).

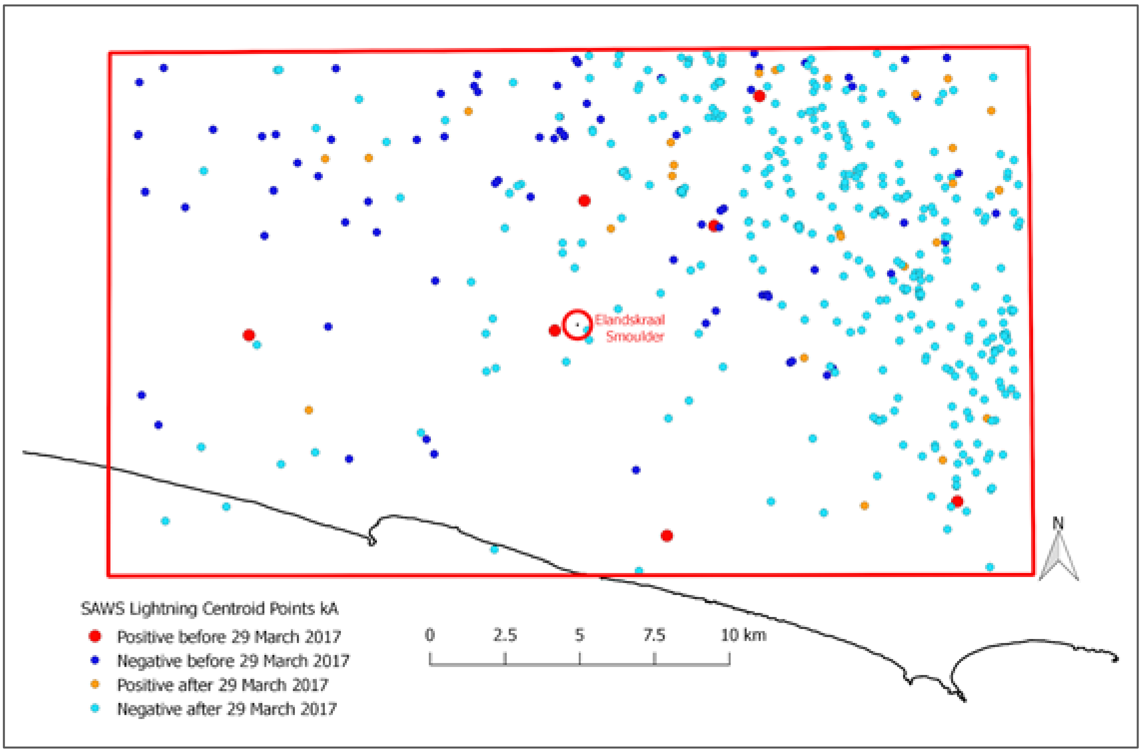

Figure 13: Centroids of estimated locations of lightning strike (99% confidence ellipses) as detected by the SAWS SALDN for period 1 Jan 2017 - 7 June 2017 around Elandskraal. The colours of the points indicate the polarity of the strike and the dates before or after 29 March 2017 (when the vegetation anomaly was detected).

The location of a detected lightning strike cannot be determined with absolute accuracy. The accuracy of the position of a lightning strike is calculated as a 2D confidence ellipse based on a Gaussian model

(Cummins, 1998). Each lightning strike has its own unique confidence ellipse which is determined by several factors including, time, latitude, longitude, peak kA, chi-square, ellipse semi-major, ellipse semi-minor, ellipse angle, degrees of freedom and number of sensors in detection (Grant *et al.,* 2011). The ellipse represents a 99% confidence that a lightning strike occurred somewhere inside the ellipse. The ellipse is therefore the equivalent of the "margin of error" for the location of each lightning strike (Vaisala user guide).

Numerous studies have confirmed the importance of long-continuous current (LCC) within lightning strikes as the main cause of ignition in forest fires (Fuquay *et al*. 1972, 1979, 1982). Lightning discharges with continuing current of 40 milliseconds or more are called long-continuing current discharges (Fuguay, 1972). The longer the energy discharge remains on the surface, the higher the probability of ignition. Studies have shown that approximately 10% of negative lightning strikes and 90% of positive lightning strikes contain LCC (Shindo and Uman 1989)**.** The probability of a strike igniting a fire depends on the presence and duration of the LCC and how receptive the fuel is to igniting, with fuel moisture playing a prominent role (Latham and Schlieter, 1989)**.**

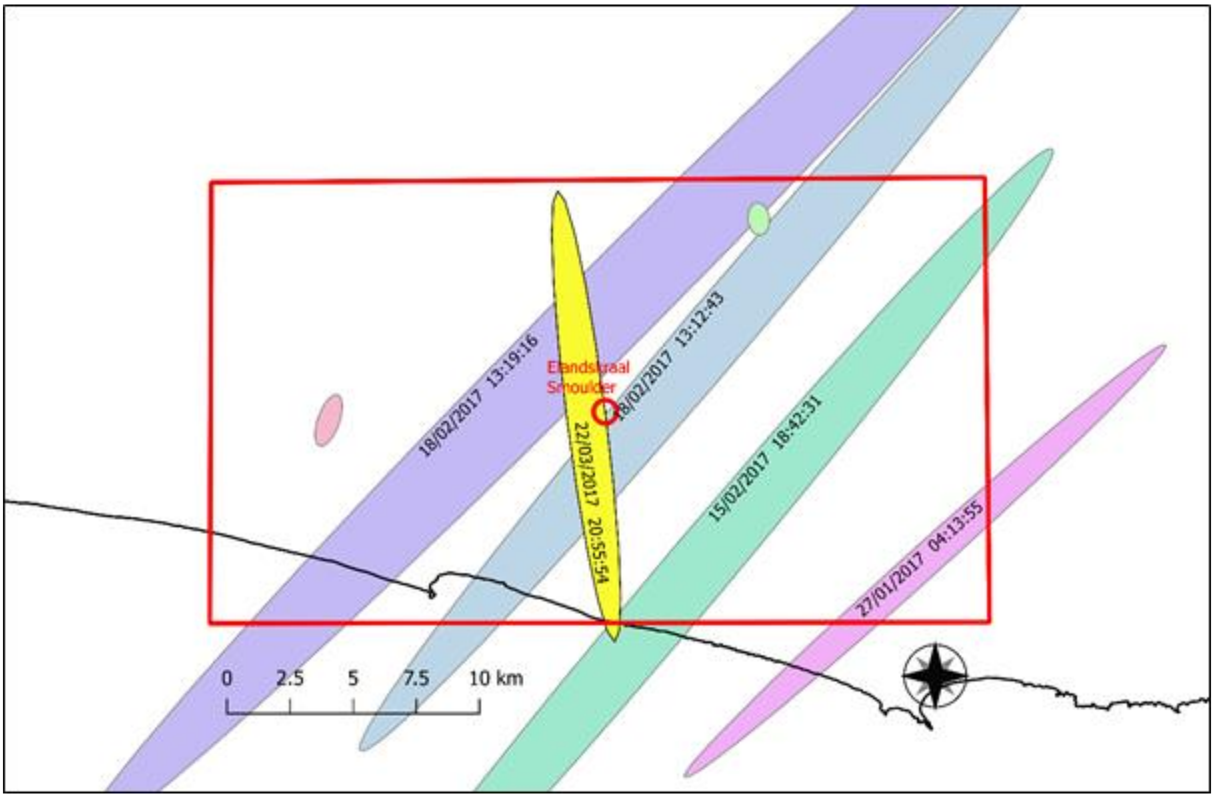

Figure 14: Positive lightning strike ellipses with a 99% confidence level for greater Knysna region and Elandskraal area between 1 Jan 2017 and 29 March 2017.

Based on the evidence of an anomaly first observed in the vegetation on 29 March 2017 and subsequent decrease in vegetation greenness as detected by the Sentinel-2 satellite, only lightning data for the period 1 Jan 2017 to 29 March 2017 were further evaluated. Given the existence of a vegetation anomaly starting on 29 March 2017, as well as the hypothesis that a positive lightning strike may have been responsible for igniting a smouldering fire, seven lightning strikes were further evaluated. Figure 14 depicts the 99% confidence ellipse for each of the seven positive lightning strikes detected between 1 Jan 2017 and 29 March 2017.

Two positive lightning strikes were detected within the proximity of the vegetation anomaly detected on 29 March 2017. The first strike took place on 18 February 2017 at 13h12 pm while the second strike took place on 22 March 2017 at 20h55 (Figure 15). Since no vegetation anomalies were observed in the Sentinel-2 EVI time series in the Elandskraal area after the 18 February 2017 lightning strike, it was not considered to be a potential cause of ignition of the smouldering patch of vegetation.

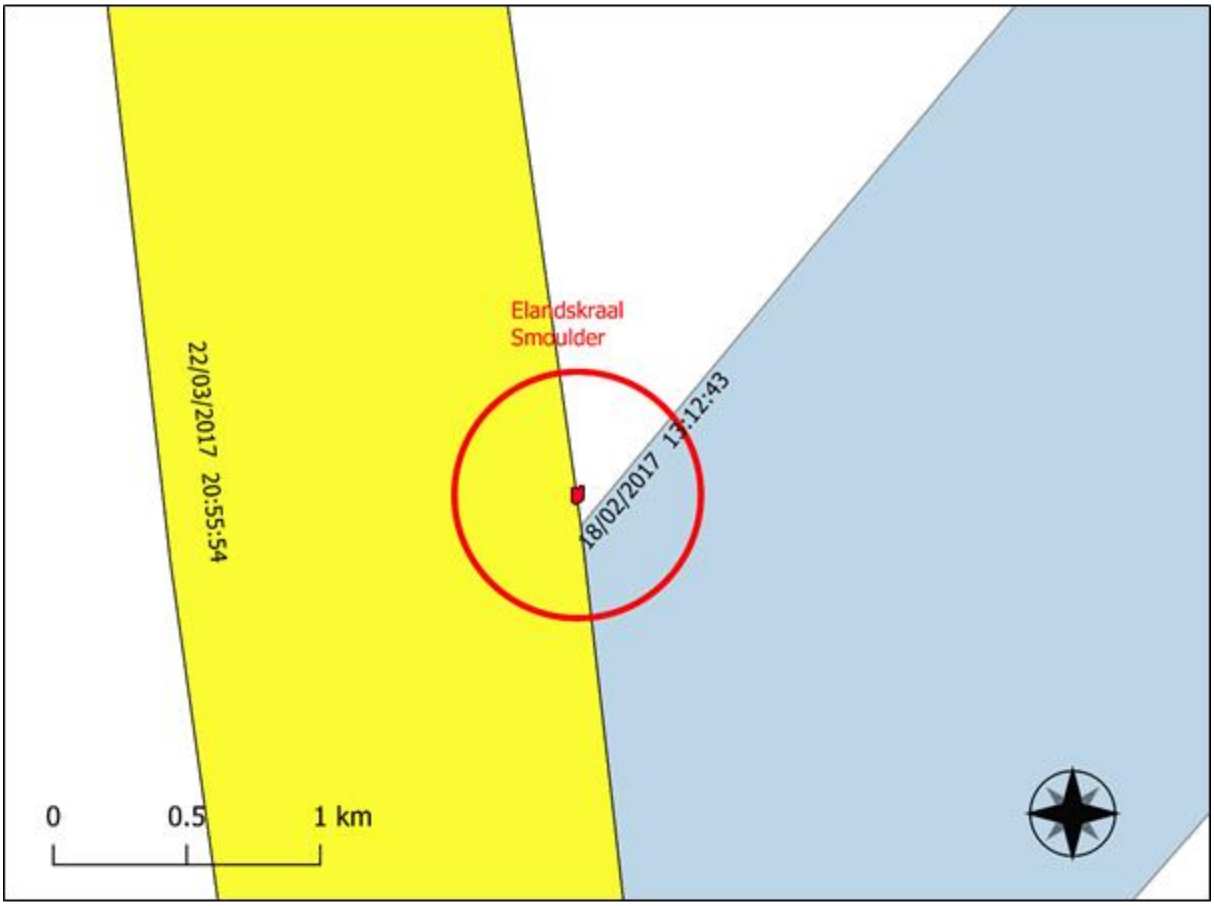

Figure 15: Positive lightning strike ellipses with a 99% confidence level area for 18 February and 22 March 2017 in relation to the site of smouldering vegetation in Elandskraal area.

The vegetation anomaly detected in the Sentinel-2 satellite imagery is located within the 99% confidence ellipse provided by SAWS for the lightning strike of 22 March 2017 detected at 18:55:54 GMT (20:55:54 SAST) (Figure 16). Therefore, the positive lightning strike of 22 March 2017, had the highest probability of all the strikes to ignite the smouldering patch of vegetation. The lightning strike on 22 March 2017 would also explain why no vegetation anomaly was observed in the Sentinel-2 EVI on 19 March 2017, but observed in the data from 29 March 2017 (Figure 9 b-e).

Figure 16: Location of smouldering patch of vegetation (yellow) within the 99% confidence ellipse (red) of the 22 March 2017, provided by SAWS.

4.2.5 "Holdover" fires

The appearance of smouldering vegetation after a lightning strike is known in the USA and Canada as a "*holdover fire*" or "*sleeper fire*". Holdover fires are slow, low-temperature, flameless fires that spread both horizontally and vertically through organic layers or roots depending on the vegetation and soil structure. Once ignited they are extremely difficult to extinguish and can persist for long periods of time underground (Rein *et al*., 2008).

The three elements necessary to start and sustain a fire as described by Moritz *et al.* (2005) are: (i) oxygen (air) - to start and sustain combustion; (ii) fuel - to sustain and/or carry flames; (iii) heat - to raise fuel temperatures to their ignition point and to ignite fuels. A holdover fire in a smouldering phase has enough fuel and heat but lacks the oxygen required to develop into a flaming front (Rein *et al*. 2008).

Lightning has the potential to trigger an ignition, generally within a dry forest floor, that survives by smouldering within organic layers for days, weeks or months until conditions favour flaming combustion, at which point the fire bursts into flames and is considered to have arrived. Thermodynamic conditions such as an increased oxygen supply (strong winds) has the potential for a smouldering combustion to transition into a flaming combustion or flare-up (Bertschi *et al*., 2003).

Holdover fires are not frequently observed in the Southern Cape due to the relatively low lightning flash densities (<2 flashes/km^2/year) and higher fine fuel moisture content of the litter layers that does not sustain smouldering (van Wilgen, 1982). Under severe drought conditions however the risk for holdover fires increases significantly due to a decrease in fuel and soil moisture content (Granger, 1984). Once a lightning strike hits a dry north-facing transformed fynbos stand with enough LCC, smouldering ignition of the material on the forest floor can occur (Latham and Schlieter, 1989). With the onset of berg wind conditions (gusty hot, dry air) enough oxygen is potentially provided to an oxygen starved holdover fire to flare-up and this sometimes results in devastating wildfires (Tyson, 1964; van Wilgen, 1984a).

Currently, very little is known about the quantities and characteristics of holdover fires in the different South African biomes (Horne, 1981). South African National Parks (SANParks) reported a lightning fire that burned large areas of fynbos and commercial timber plantations in the Tsitsikamma area in 2005[11]. In countries such as the USA and Canada holdover fires are responsible for millions of hectares of area burned annually (Anderson, 2002). Various probabilistic models have been developed in Canada and the US to quantify the risk of lightning strike ignitions within fine fuels and organic layers (Wotton *et al.,* 2005). These models have become invaluable to detect possible holdover fires early and to allow fire services to manage the risk.

The vegetation anomaly observed from 29 March 2017, coupled with the detected positive lightning strike of 22 March 2017 suggests that the smouldering vegetation seen in the drone footage of 27 May 2017 could have been produced by a holdover fire on the forest floor underneath the dry vegetation canopy in Elandskraal.

4.2.6 Weather before the fire

The Western Cape experienced an unusually severe Atlantic storm on 6 June 2017 preceded by a week of dry windy conditions. Winter storms are anticyclonic weather systems that result in the low-pressure systems travelling north-east from Cape Town and passing slightly north of the Garden Route. This deflection towards the north of the Garden Route creates a north-westerly wind into the region which results in hot dry air known as a “berg wind” (Tyson, 1964).

A berg wind develops when descending air heats up to approximately 32°C - 38°C over the Outeniqua Mountain Range, in this case, while moving towards the coast. In addition to being hot, the air is extremely dry. Berg wind conditions are synonymous with high fire danger ratings (Geldenhuys 1994). The winds dried and wilted vegetation in the area that was already stressed due to severe drought. The Lowveld Fire Danger Index (LFDI) (Meikle and Heine, 1987) is a fire weather index that describes the risk of a fire becoming uncontrollable. The LFDI is calculated based on air temperature, relative humidity and wind speed. Berg wind conditions are synonymous with high LFDI values. LFDI readings were in the “Very High” (orange) and “Severe” (red) fire danger categories on 30 and 31 May as well as 3, 4 and 6 June as illustrated in Figure 17.

[11] Source: https://www.sanparks.org/assets/docs/parks_grnp/about/monitoring-summary.pdf, accessed: March 2018

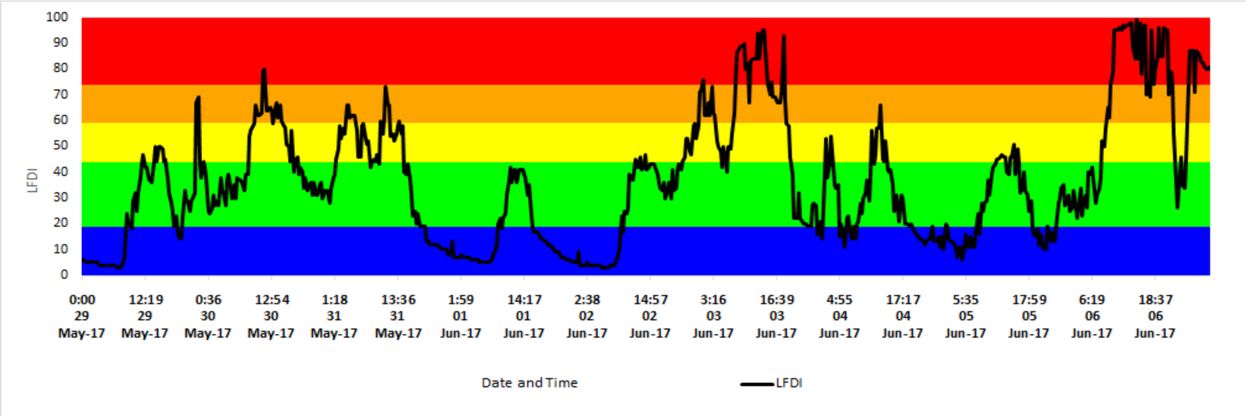

Figure 17: Lowveld Fire Danger Index (LFDI) at Kooigoed weather station (33.9628 S, 22.855 E) from 29 May 2017 to 7 June 2017.

4.3 Start of the fire

The three main factors that influence fire behaviour and severity form the *fire behaviour triangle* as described by Countryman (1972) and Moritz *et al*. (2005): (i) weather - windy conditions can increase oxygen supply; (ii) fuel - sustains and/or carries the flames; (iii) topography - terrain, slope and aspect.

4.3.1 Weather on 7 June 2017

A private weather station at Kooigoed (33.9628 S, 22.855 E, about 1.4 km south-east of the smouldering area/holdover fire), recorded the temperature, dew point, relative humidity, wind direction and wind speed during the early hours of the 7 June 2017 (Figure 18). Salient features of the weather during this time period are highlighted below.

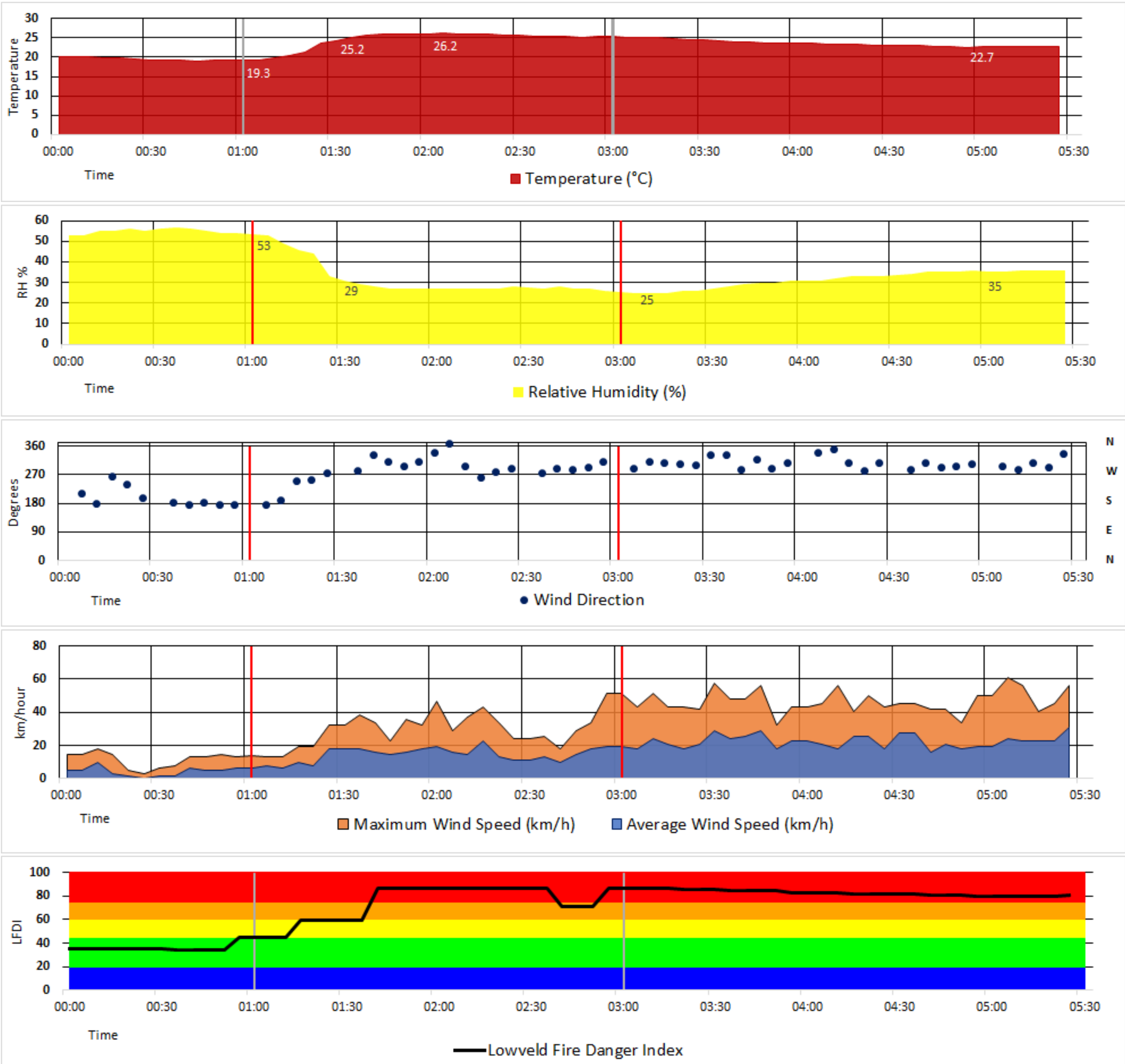

Figure 18: Weather parameters as measured on 7 June 2017 by Kooigoed weather station located 1.4 km south-east of the holdover fire (33.963 S, 22.855 E). Red vertical lines indicate significant changes in weather conditions.

Significant Weather observations on 7 June 2017 (Figure 18):

00h00 - 01h00: Predominantly southerly winds blowing at less than 5 km/h with no indication of berg wind conditions. Relative humidity above 50% and overall "Low to Medium" LFDI fire danger observed.

01h00 - 01h30: Signs of berg wind conditions emerge with a sudden shift in wind direction from southerly to westerly winds at around 01h09. Average wind speeds increase from 5 km/h to 20 km/h with wind gusts of more than 30 km/h. A significant rise in the air temperature from 19°C to 25°C and a drop in humidity from 53% to 29% within a period of 20 minutes was recorded raising the LFDI from "Medium" to "Very high" fire danger.

03h00 - 05h23: North-westerly berg winds from the Outeniqua Mountains reduced the relative humidity further to only 25%. The most significant change in the weather conditions from 03h00 was an increase in the speed of wind gusts from 25 km/h to over 40 km/h. Gusts up to 50 km/h were recorded at 03h30 and up to 60 km/h at 05h10 with a 55 km/h gust recorded at 05h23 when the weather station stopped functioning.

4.3.2 First detection of the Elandskraal fire

The first detection and initial spread of the Elandskraal fire was examined in chronological order using the available satellite data and a Bushnell motion-sensing camera system which captured photographs during the morning of 7 June 2017. The timeline of various satellite detections and photographs taken by the Bushnell motion-sensing camera is given in Figure 19.

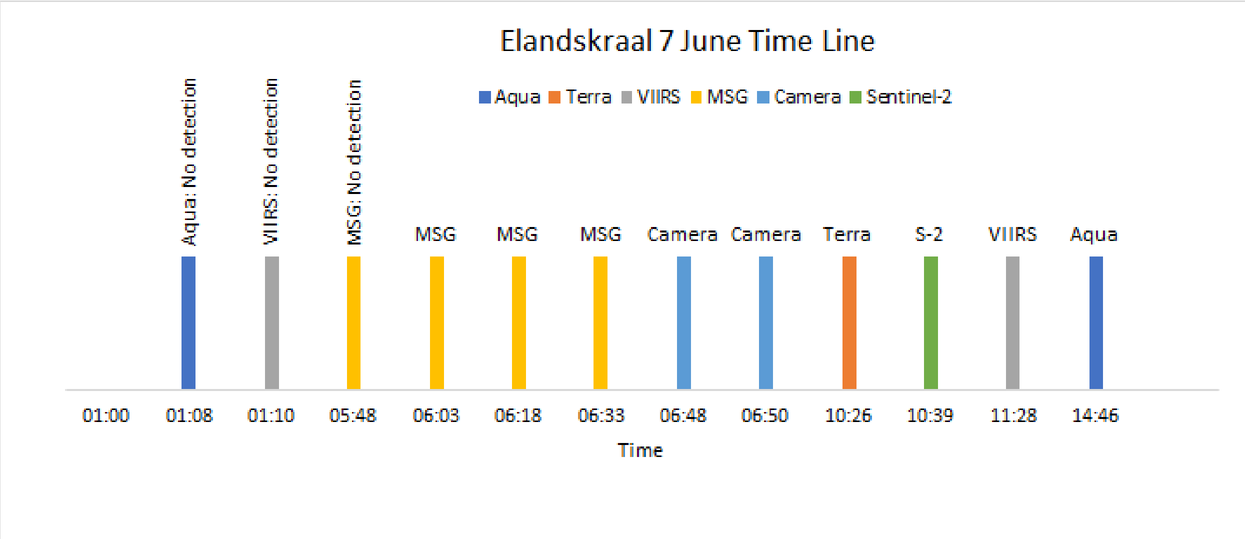

Figure 19. Timeline of active fire detections by satellite sensors and Bushnell motion-sensing camera on 7 June 2017.

Three different satellites captured thermal data over the Elandskraal area between 01h00 and 06h00 on the 7 June 2017 (Table 1). Aqua MODIS (NASA) and NPP VIIRS (NOAA) formed part of the polar orbiting satellites that captured data over the Knysna area around 01h10. The SEVIRI sensor on the MSG geostationary satellite provided updated thermal scans of the area every 15 minutes. In addition to the active fire products derived from the Aqua MODIS (Gigio *et al*, 2016) and NPP VIIRS[12] satellites, night time reflectance data from the NPP VIIRS Day/Night Band at 01h10 was also included in the analysis. The NPP VIIRS Day/Night Band detects natural and anthropogenic night-time light emissions from sources such as city lights, lightning, auroras, fires, gas flares, and fishing fleets.

01h08 - 01h10: The active fire data captured by Aqua MODIS at 01h08 and NPP VIIRS at 01h10 showed no indication of a fire at Elandskraal (Figure 19). The NPP VIIRS Day/Night band (Figure 20) detected a fire at Uniondale, 40 km to the north-east of Elandskraal, indicated by illuminated cloud cover, but it did not show any sign of a fire close to Elandskraal at 01h10.

[12] Source: https://viirsland.gsfc.nasa.gov/PDF/VIIRS_activefire_User_Guide_v1_3.pdf, accessed: March 2018

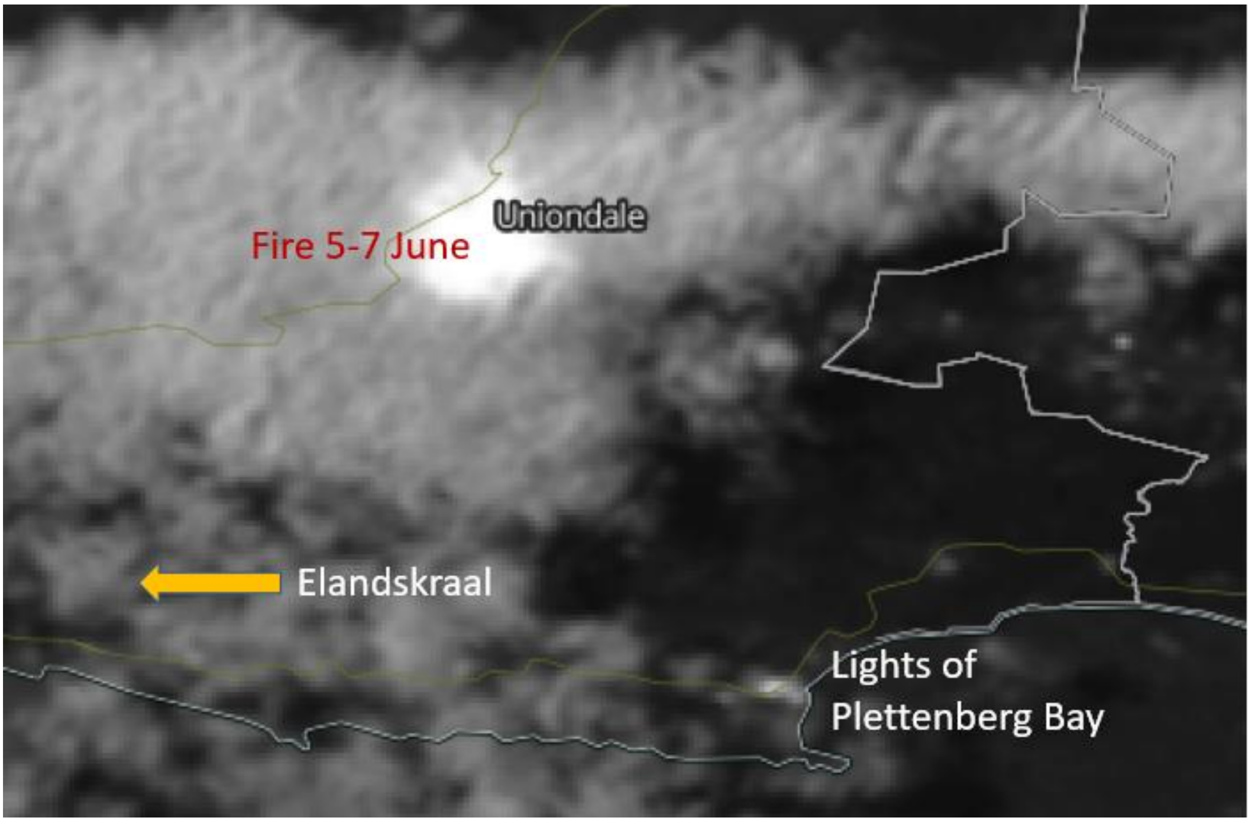

Figure 20. NPP VIIRS Day-Night band showing fire near Uniondale at 01h10 on 7 June but no detectable fire at Elandskraal.

04h03: The Kruisfontein fire to the east of Knysna was detected by MSG at 04h03 on the morning of 7 June 2017 (Figure 21a). This fire continued to grow while there were no fire detections with MSG in the Elandskraal area up until 05h48 (Figure 21b and Figure 21c).

06h03: The MSG scan segment at 06h03 identifies a thermal anomaly across two adjacent pixels in the Elandskraal area. The anomaly grows in size and intensity with every subsequent 15 minute MSG scan confirming the anomaly to be an active fire. Based on the minimum detectable fire size (Figure 4) an area of approximately 1-2 ha was actively burning at 06h03 (Figure 21d). The Elandskraal fire continues to grow from 06h23 (Figure 21e) and the extent of both fires is illustrated at 10h39 (Figure 21f) which coincides with the Sentinel-2 image of the fire at the same time on 7 June 2017.

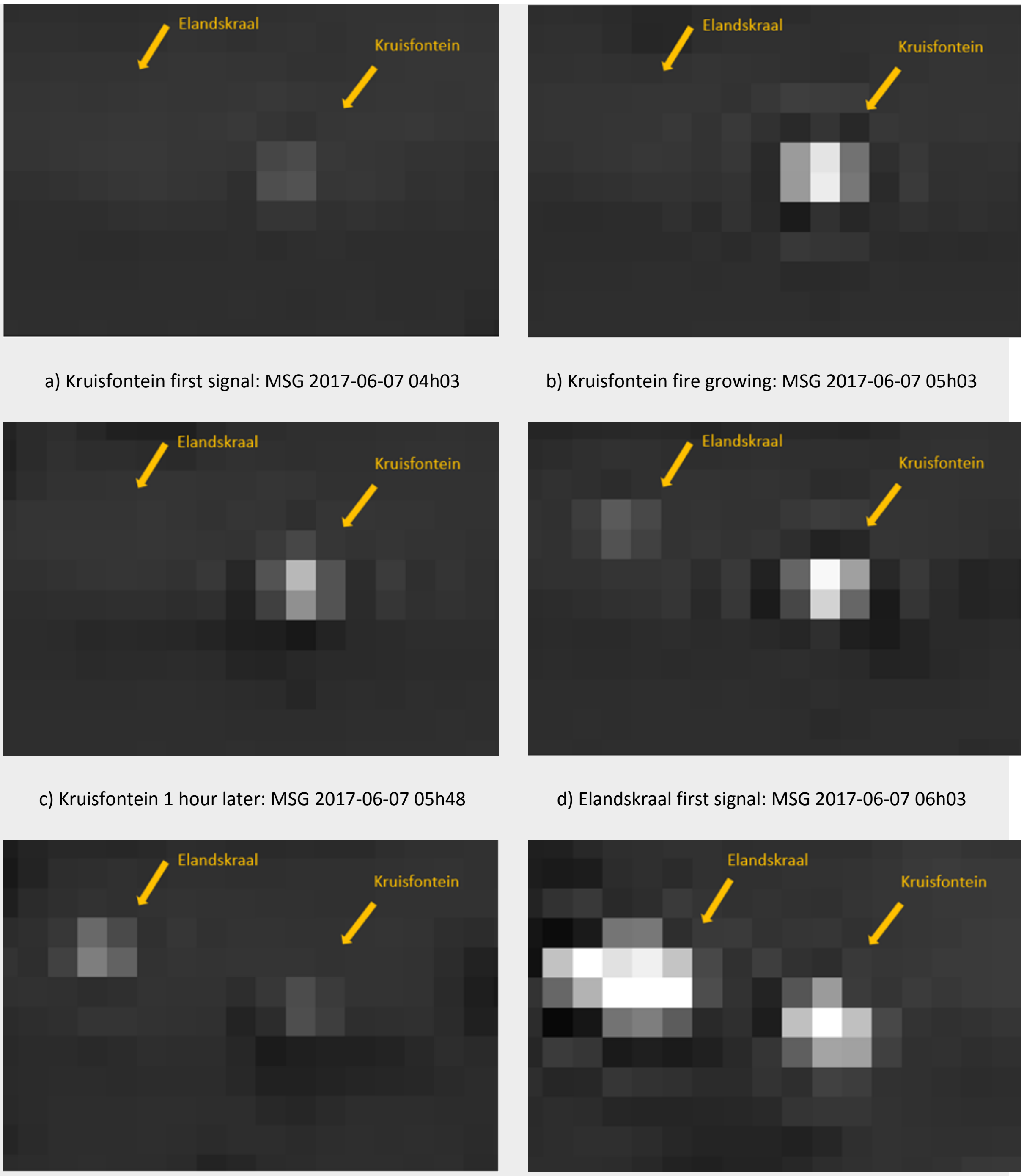

a) Kruisfontein first signal: MSG 2017-06-07 04h03

b) Kruisfontein fire growing: MSG 2017-06-07 05h03

c) Kruisfontein 1 hour later: MSG 2017-06-07 05h48

d) Elandskraal first signal: MSG 2017-06-07 06h03

e) Elandskraal 15 minutes later: MSG 2017-06-07 06h23

f) Fires at time of Sentinel-2 overpass: MSG 2017-06-07 10h39

Figure 21. Radiance of active fires detected by MSG satellite in the early hours of 7 June 2017 showing the sequence of fire spread.

4.4 Initial spread of the fire

Berg wind conditions were observed from 01h09 (see Section 4.1) with westerly to north-westerly strong winds blowing between 03h00 and 05h23, at which time the weather station stopped functioning. If the holdover fire flared-up under the prevailing north-westerly winds, the fire would have moved up the slope towards the croquet lawn and homestead located at the top of the hill about 524 m to the south-east (Figure 22).

Figure 22. The croquet lawn, circled in red, with wind direction at 05h00 indicated by white arrows.

Drone footage (Figure 23) captured on the morning after the Elandskraal fire (8 June 2017) shows damage to the croquet lawn and the buildings. The kikuyu grass on the croquet lawn was burned on the north-west, north and western sides of the lawn with little to no damage on the southern sides. The burn pattern on the grass shows that the direction of the fire was in line with the wind direction measured by the weather station at Kooigoed after 03h00 on the morning of the fire.

Figure 23. The burn scar visible on the croquet lawn as observed by drone footage on 8 June 2017 affected from the north-west .

The WorldView-3 satellite imagery in Figure 24 confirms the geographic location and direction of the croquet field in relation to the wind.

Figure 24. The WorldView-3 burned area imagery used to confirm that the north-westerly wind would affect the burn pattern on the croquet field as shown.

4.4.1 Spread to Kooigoed

A Bushnell motion-sensing camera was mounted at a structure referred to as Kooigoed approximately 1.4 km from the holdover fire. It captured photographs of the approaching fire. The Bushnell motion-sensing camera was first activated at 06h48 and captured burning vegetation close to the structures, approaching from the west (Figure 25). This time-stamped photograph was essential to estimating the initial rate of spread. Images captured minutes later show flames and flying debris crossing the Bushnell motion-sensing camera's field of view. The Bushnell motion-sensing camera survived the first fire front and continued to capture 440 images before it melted at around 09h14 due to a second fire front.

(a)

(b)

(c)

Figure 25. Photographs captured by Bushnell motion-sensing camera at Kooigoed triggered at a) 06h48, b) 06h50 and c) 06h52 on the morning of the 7 June 2017.

4.4.2 Estimated rate of spread

The Elandskraal fire spread in a south-easterly direction towards Kooigoed where it was first detected at 06h48 by the Bushnell motion-sensing camera. The accuracy of the time recorded by the Bushnell motion-sensing camera was validated by noting the time of sunrise in the previous day's photographs.

The MSG satellite detected first evidence of a potential fire at 06h03 on 7 June 2017. Based on the minimum area a fire has to cover in order to be detected by two MSG pixels (Figure 21d), an area of approximately 1-2 ha must have been actively burning at 06h03 (Figure 26). The estimated distance between the edge of the 1-2 ha active fire and the croquet lawn is 351 m, while the distance from the croquet lawn to Kooigoed is approximately 1082 m.

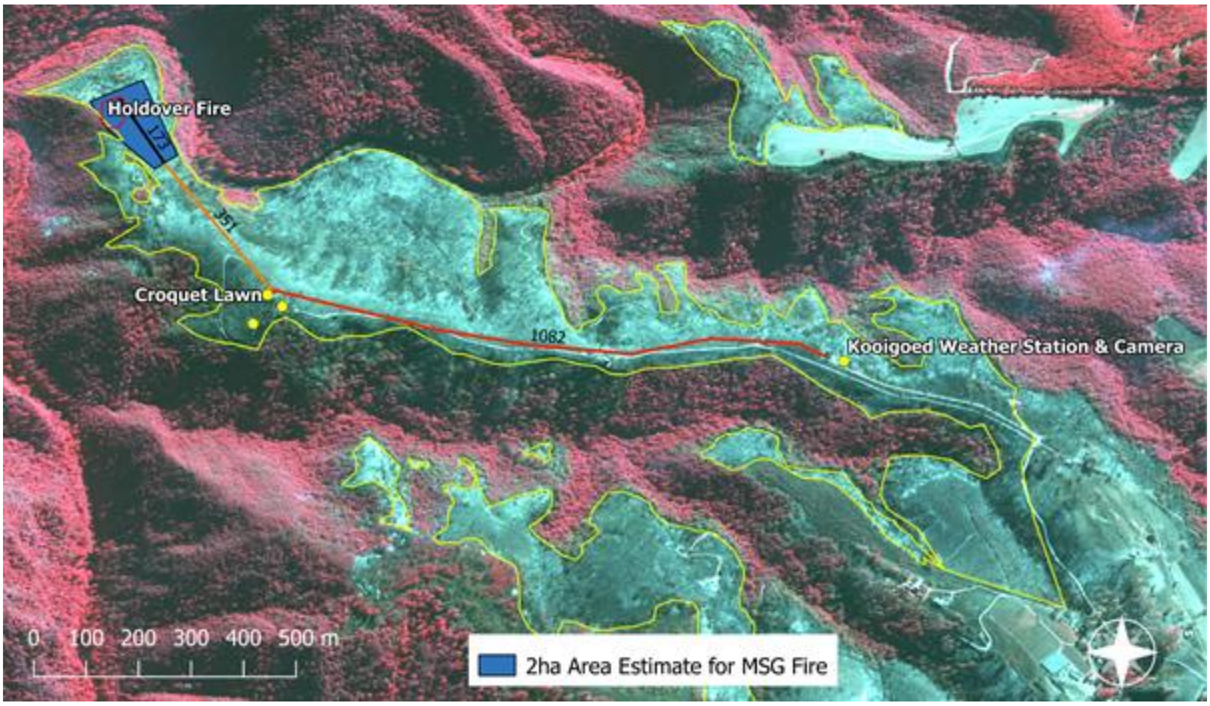

Figure 26. Distances between relevant points in the burned area showing the estimated 1-2 ha fire registered by the MSG satellite (dark blue polygon) at 06h03. Burned area (light blue shades outlined in yellow) was mapped with WorldView-3.

The exact number of minutes the fire took to grow to a size of 1-2 ha is not certain, but the time of detection of the fire once it reached an estimated 1-2 ha size is confirmed at 06h03. The time difference between the confirmed fire detection at 06h03 and the spread of the fire to Kooigoed (06h48) is 45 minutes. The distance from the south-eastern edge of the 1-2 ha area taken as the estimated fire front, to the Bushnell motion-sensing camera location at Kooigoed is approximately 1 433 m, and thus the mean rate of spread (ROS) was calculated at 31.8 m/min based on these sensor observations. Taking the prevailing wind direction and topography into account, the head fire would have moved rapidly from the original smouldering area to the croquet lawn (Figure 26) as it was directly aligned with the north-westerly wind and up-slope. Kooigoed is 1 082 m east of the croquet lawn and strong north-westerly winds would have driven a slower moving flank fire towards Kooigoed. The mean rate of spread falls well within the previously published expected ROS for Fynbos of between 2.4 m/min and 53.4 m/min as recorded by van Wilgen *et al.* (1985).

An estimate of the flare-up time of the Elandskraal fire can also be inferred using the start time of the Kruisfontein fire. The Kruisfontein fire was reported by a MTO Kruisfontein Plantation fire lookout tower at 03h30 with MSG first observing the thermal anomaly first at 04h03 (Figure 21a). The satellite detected a potential active fire across two pixels suggesting that an estimated area of 1-2 ha was burning at that time. If it is assumed that the fire was reported within 10 minutes of the start, it would have taken the fire 43 minutes to reach the size of 1-2 ha in order to be detected. Once again, assuming that the prevailing weather and fuel conditions were similar to that for the Elandskraal fire that was detected at 06h03, it may be deduced that the Elandskraal fire could have started approximately 43 minutes before it was detected by the MSG satellite. This suggests an estimated starting time of the Elandskraal fire at 05h20.

4.4.3 Rothermel fire spread model simulation

The potential flare-up time of the Elandskraal fire was also estimated through a simulation using the Rothermel Fire Spread model which has previously been successfully applied in Fynbos fuel types (van Wilgen *et al.*, 1985). The model has recently been integrated within the new AFIS fire behaviour module available to fire managers through the fire dashboard. The Rothermel fire spread model (Rothermel, 1972) is widely used in the USA and Canada to simulate the forward rate of spread (ROS) at the head of a surface fire (Sullivan, 2009), and is the primary fire spread model of many fire prediction systems (Lopes *et al.*, 2002; Sullivan, 2009; Finney *et al.,* 2011*)*. In the Rothermel model, ROS is simulated as a function of topography, weather and a "fire behaviour fuel model" (hereafter: fuel model) that consists of a number of fuel parameters for a given fuel complex (Albini, 1976; Burgan and Rothermel, 1984). The aim of the Rothermel model simulation was to (i) determine an estimated holdover flare-up time, (ii) estimate ROS and (iii) test if the burn pattern predicted by the fire spread model was similar to the final mapped burn scar when the holdover fire location was used as an ignition point in the model. The simulated ROS could be compared to the ROS of 31.8 m/min that was calculated between the MSG satellite detected fire and the Kooigoed Bushnell motion-sensing camera detection.

In this case the input variables included; (i) the start point at the location of the holdover fire, (ii) the average weather conditions (temperature, relative humidity, wind speed and wind direction) as recorded by four observations at 05h01, 05h06, 05h12 and 05h17 at the Kooigoed weather station, (iii) topography represented by a 30 m digital elevation model (Shuttle Radar Topography Mission - SRTM) and (iv) the Chaparral Fuel Type which is a closer match to the scrub forest existing in the site than the fynbos fuel type model developed by Van Wilgen (1984b).

The result of the model simulation indicate that the head fire would have reached Kooigoed in approximately 93 minutes based on average weather conditions between 05h00 and 05h20 and taking the holdover fire location as the ignition point (Figure 27). Deducting 93 minutes from the arrival time of the fire at Kooigoed (06h48) as observed by the Bushnell motion-sensing camera would indicate a start of the flare-up at approximately 05h15.

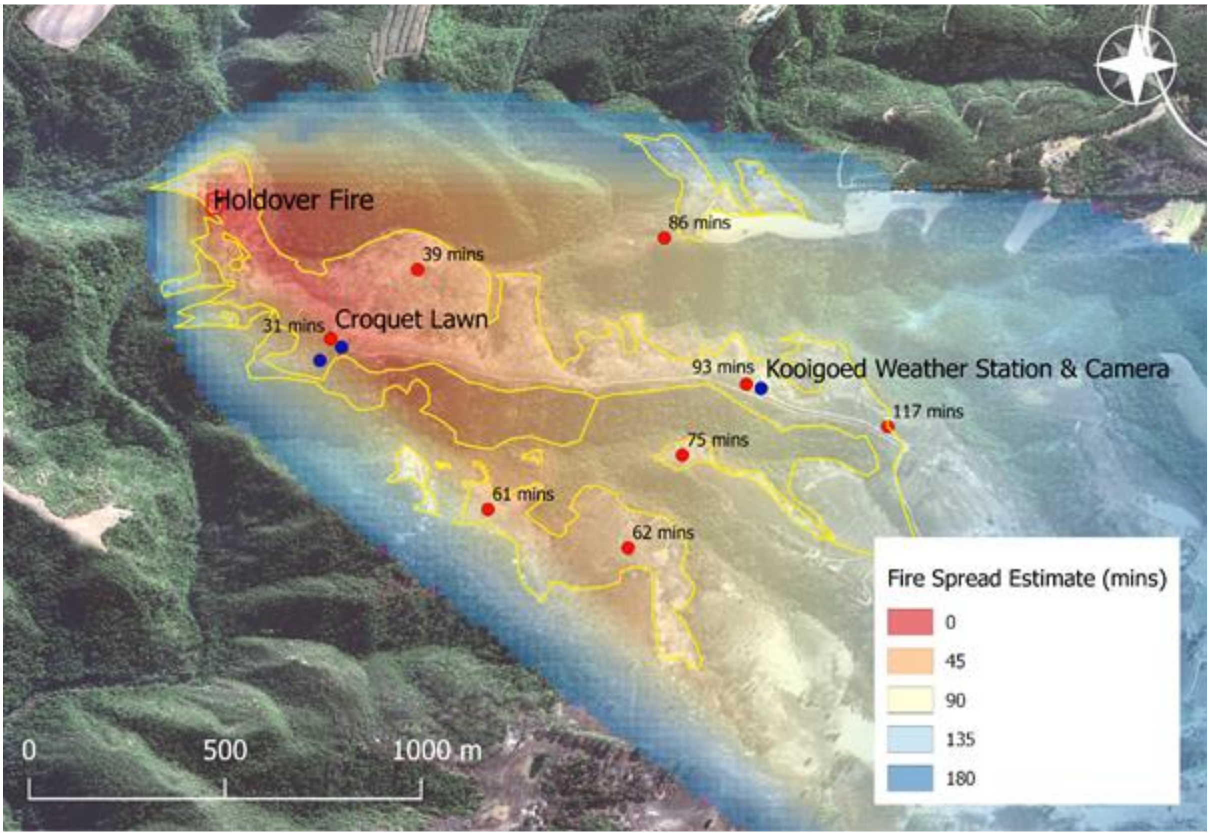

Figure 27. Rothermel Fire Spread Model output based on the starting point at the location of the holdover fire, topography and average weather station data from 05h01, 05h06, 05h12 and 05h17 (RH% = 36; Ave Wind Speed = 23 km/h; Wind Direction = 242^0). The time (in minutes) the fire would take to reach each pixel is indicated by the colour of the pixel and by the number given next to points of interest (red points). The burned area extent mapped from Sentinel-2 imagery is overlaid in yellow.

The sensor-observed ROS of 31.8 m/min calculated between the MSG fire detection (06h03) and Kooigoed Bushnell motion-sensing camera timestamp (06h48) was comparable to the Rothermel model's calculated average ROS of 20 m/min along a path between the holdover fire and Kooigoed (standard deviation of 9 m/min; minimum 3 m/min and maximum 41 m/min)(Figure 27). The Rothermel model calculations were based on average wind conditions (Ave Wind Speed = 23 km/h; Wind Direction = 242^0) and the model does not take the effect of wind gusts into account. Wind gusts which were measured between 40 km/h - 60 km/h around 05h20 (Figure 18) would have significantly increased the ROS of the fire, as well as the amount of spotting towards neighbouring areas to the south-east. This may explain why the Rothermel model's average ROS is 10 m/min slower than the ROS calculated between the MSG detection and the Kooigoed Bushnell motion-sensing camera detection.

The fire spread pattern predicted by the Rothermel model contained the full extent of the burned area mapped with the Sentinel-2 satellite image in the Elandskraal area (yellow outline) (Figure 27). The model results lends support to the theory of the holdover fire as the ignition location, as well as an estimated flare-up time between 05h00 and 05h20 based on the prevailing weather conditions. The modelling approach may be used to further explore the predicted fire spread patterns under alternative scenarios, including different ignition locations, start times and weather conditions.

4.4.4 Influence of topography

The impact of topography on fire behaviour is mainly determined by slope, aspect and terrain. Topographic variations has the potential to result in dramatic changes in the behaviour of a fire over a terrain (Countryman, 1972). In the case of the Elandskraal fire the topographic setting of the smouldering vegetation potentially had a very large influence on the behaviour of the fire.

The topography of the Elandskraal area is shown in Figure 28b. The spot heights near the origin of the holdover fire range in altitude from 173 m to 175 m above mean sea level. The floor of the Karatara River in this location is approximately 35 m above mean sea level. The spot heights to the north of the smouldering hillside are just over 200 m in altitude which means that the north-westerly berg winds would be moving from a higher elevation to a lower elevation. This is conducive to the formation of an eddy wind in the valley as described by Geldenhuys (1994) (Figure 28a & Figure 28b). The location of the original smouldering area in relation to the surrounding topography and the direction of strong berg winds suggests that an eddy could have developed that initially trapped the fire for a period of time before it escaped and started spreading in a south-easterly direction (Figure 28a & Figure 28b) (Geldenhuys, 1994). This potential eddy-effect may prevent more precise estimations of the time of flare-up and initial ROS of the fire between 05h00 and 05h30.

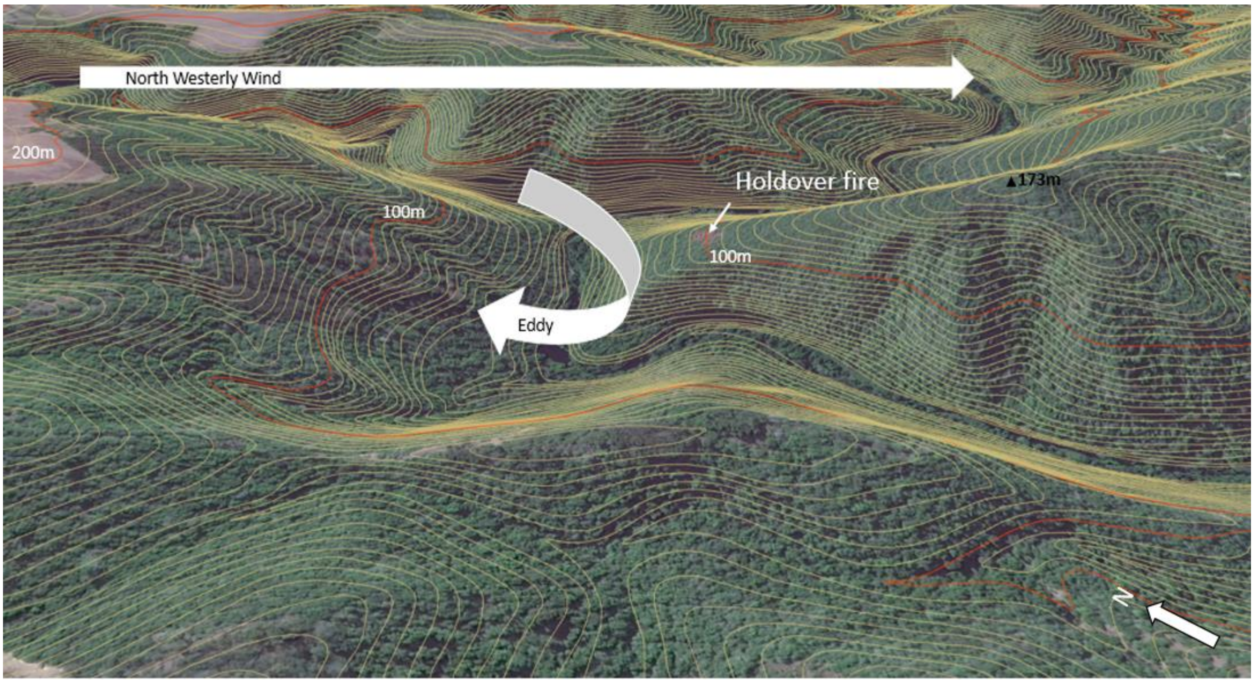

Figure 28a. Oblique view of north-westerly wind flow and wind eddies forming in the valley on the lee side of the hill at 200 m altitude.

Figure 28b. Overhead view of north-westerly wind flow and wind eddies forming in the valley on the lee side of the hill at 200 m altitude.

4.4.5 Spotting

During strong berg winds, wildfires can create powerful updrafts in the form of convection columns, which can launch burning plant materials such as pine cones and protea flowers into the air (Geldenhuys *pers comm.*, 2017). Heat and moisture exchanges occur between the fire, the convection column and the atmosphere, resulting in the formation of new fire-driven wind and convective updrafts. Burning material is then transported by the wind flow, simultaneously combusting, until it lands on the ground. Depending on the weather and fuel conditions where these burning embers (material) land, they may ignite the fuel and start a new fire. Such a fire is called a spot fire, and the process is called spotting (Martin *et al*. 2016).

Evidence of spot ignitions can be seen on the burn scar map produced from the 30 cm resolution WorldView-3 imagery of 19 June. These point ignitions (the V-patterns seen in Figure 29) are visible on many of the north- and west-facing slopes along the main fire front and corresponding with the predominant north-westerly wind direction. Spot ignitions only cause V-patterns where the vegetation can sustain a crown fire hence no V-patterns are visible on the moist southern slopes even though understory burning is possible.

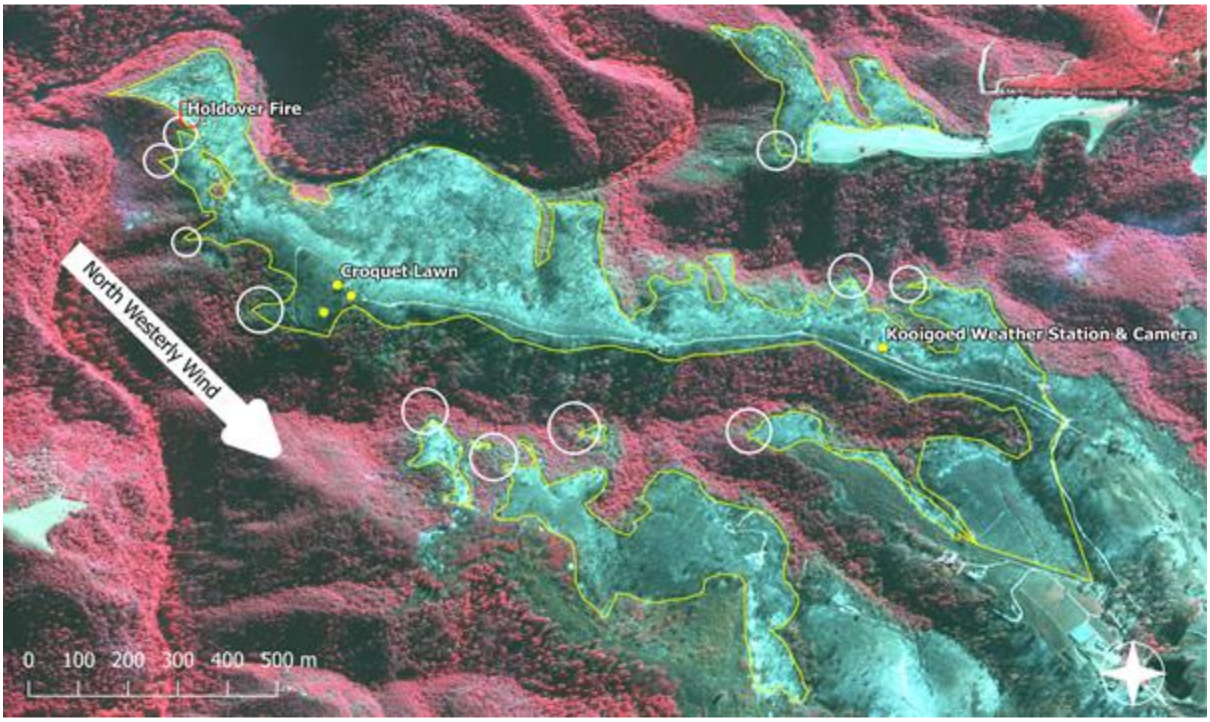

Figure 29. Burn scar mapped from WorldView-3 imagery of 19 June 2017 (yellow outline), showing examples of V-shaped point ignitions probably related to "spotting" by the fire (white circles).

4.5 After the Fire

4.5.1 Activation of the International Charter for Space and Major Disasters

The International Charter for Space and Major Disasters is an International Agreement between nations that allows for rapid access to high resolution satellite imagery from various space agencies and commercial satellite operators during and after a disaster. Upon activation, space agencies and commercial satellite operators task their satellites to capture imagery over the disaster area for two week period in support of relief efforts. The CSIR assisted the National Disaster Management Centre (NDMC) in the activation of the charter and directly supported the Western Cape Disaster Management Centre (WCDMC) and other fire agencies through the AFIS programme and by processing the satellite data made available through the charter. The AFIS team's unique skills in the processing and production of geospatial fire products, enabled them to start a chronological, geospatial analysis of the Elandskraal fire.

4.5.2 Total burned area

A Sentinel-2 of 14 June 2017 was used to map the total burned area of the Elandskraal and Kruisfontein fires and the first estimate of burned area is 9 440 ha (Figure 30). There is an underestimation of areas that burned under forest canopies due to the remaining green tree tops that are assessed by the automatic algorithm as unburned areas.

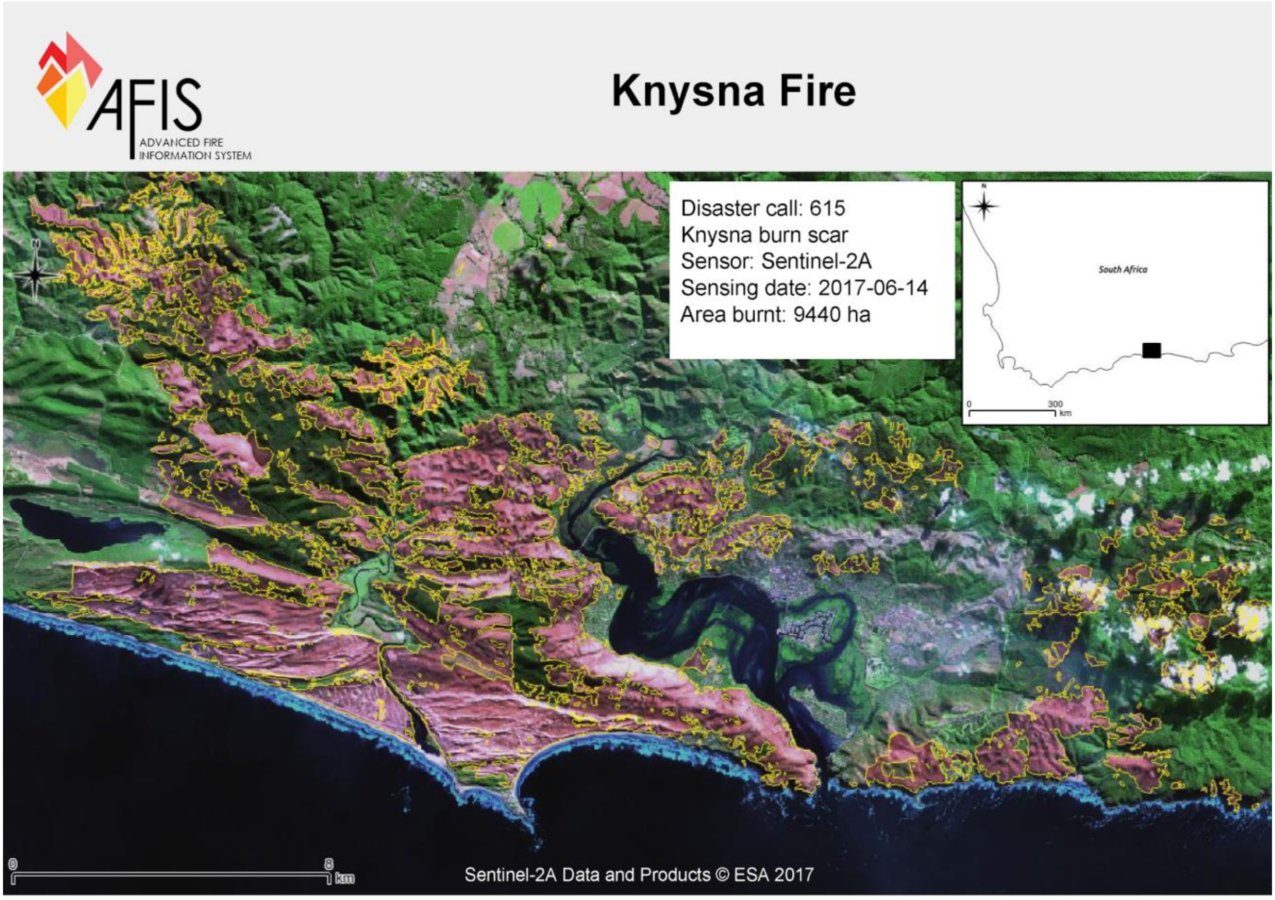

Figure 30. Burned area of the Elandskraal (west) and Kruisfontein (east) fires around Knysna displayed as a yellow outline on the Sentinel-2 images of 14 June 2017. The burned area is visible in shades of pink and remaining vegetation in shades of green.

5 SUMMARY AND CONCLUSIONS

This analysis demonstrates the value of geospatial multiple sensor data combined with domain knowledge to better understand disastrous fire events. The findings of the technical analysis can be summarised as follows:

The location of the smouldering area identified by the drone footage (27 May 2017):

- Video footage captured by a drone shows a patch of smouldering vegetation on the 27 May 2017.
- The video footage is referenced against a GeoEye-1 high resolution satellite image captured on the 20 April 2017 and the smouldering area is identified at (33.957624 S, 22.839807 E), the north-western corner of the Elandskraal burn scar. The GeoEye-1 image (20 April 2017) showing the area of brown, dying vegetation is now publicly viewable in Google Earth.

First evidence of the existence of a smouldering fire

- Knowledge of the existence and location of the smouldering patch of vegetation allowed for a time-series analysis of Sentinel-2 satellite data to determine the date when satellites first identified an anomaly in the vegetation.
- There was no sign of any decreases in the vegetation greenness on 19 March 2017 based on the Sentinel-2 Enhanced Vegetation Index (EVI).
- A small anomaly of 122 m^2 indicating a decrease in vegetation greenness was detected in Sentinel-2 image of 29 March 2017.
- The anomaly grew to a size of 3 033 m^2 by 18 May 2017 in the last Sentinel-2 image prior to the fire.
- The patch of brown, potentially dying vegetation was growing at an estimated rate of 50 m^2 per day.
- The smouldering fire observed in the drone footage of 27 May 2017 explains the patch of dying vegetation first observed on the 29 March 2017 and confirms the existence of a smouldering patch of vegetation in the north-western corner of the Elandskraal burned area.
- Sentinel-2 satellite data suggests that the ignition of the holdover fire probably occurred between the 19 and 29 March 2017.

The potential cause of the holdover (smouldering) fire

- Literature suggests that lightning may be responsible for approximately 30% of the fires in the Southern Cape region. Lightning was investigated as a potential source of ignition based on the evidence of a vegetation anomaly (decrease in greenness).
- Lightning strike data were acquired from the SAWS's South African Lightning Detection Network (SALDN) for the period 1 January 2017 to 7 June 2017 for an area of approximately 20 km X 20 km

around Elandskraal. A total of 453 strikes were detected consisting of 32 positive strikes and 421 negative strikes. Based on the evidence of an anomaly first observed in the vegetation on 29 March 2017, only lightning data for period 1 Jan 2017 to 29 March 2017 were further evaluated.

- Positive lightning strikes have the potential to cause fires due to their long continuous current (LCC) (>40 milliseconds) transfer onto the ground, which increase their probability to ignite fuel. In contrast, negative strikes have only 10% probability of causing a long continuous current.

- The location of a detected lightning strike cannot be confirmed with an absolute accuracy. Each lightning strike has its own unique ellipse of potential location (99% confidence) covering a large area.

- Two positive lightning strikes were detected within the proximity of the vegetation anomaly detected on 29 March 2017. The first strike took place on 18 February 2017 at 13h12 pm while the second strike took place on 22 March 2017 at 20h55. Since no vegetation anomalies were observed in the Sentinel-2 EVI time series in the Elandskraal area after the 18 February 2017 lightning strike, it was not considered to be a potential cause of ignition of the smouldering patch of vegetation.

- The vegetation anomaly detected in the Sentinel-2 satellite imagery is located within the 99% confidence ellipse of a positive lightning strike of 22 March 2017 detected at 18:55:54 GMT (20:55:54 SAST) (provided by SAWS). This particular lightning strike (22 March 2018) has the highest probability of all the strikes to ignite the smouldering patch of vegetation. This would also explain why no vegetation anomaly was observed in the Sentinel-2 EVI on 19 March 2017, but observed in the data from 29 March 2017.

From smouldering to flaming ignition

- The appearance of smouldering vegetation after a lightning strike is known as a “holdover fire”. Holdover fires are slow, low-temperature, flameless fires that propagate both horizontally and vertically through organic layers and roots in the ground.

- Holdover fires are not frequently observed in the Southern Cape due to the relatively low lightning flash densities (<2 flashes/km^2/year) and higher fine fuel moisture content of the litter layers that does not sustain smouldering. Under severe drought conditions, however the risk for holdover fires increases significantly due to a decrease in fuel and soil moisture content. If lightning strikes the dry north-facing slope of a transformed fynbos stand with sufficient LCC, smouldering ignition of the material on the forest floor can occur.

- For a holdover fire to flare-up (or arrive) the litter fuels need to be sufficiently dry and a significant increase of oxygen is required.

- Excessive drying of fuels due to days of berg wind conditions before the 7 June coupled with a drop in relative humidity to 25% and an increase in temperature by 5 degrees to 25 degrees between 01h09 and 03h00 ensured that the vegetation was fully cured and highly flammable.

- Strong berg winds with gusts in excess of 50 km/h recorded between 03h00 and 05h00 could have provided sufficient oxygen for the holdover fire to flare-up.

- Based on the fuel and weather conditions the probability for a holdover fire to have flared-up during the period of 03h00 - 05h23 of 7 June 2017 was extremely high.

Estimated time of ignition

- The active fire data captured on 7 June 2017 by Aqua MODIS at 01h08 and NPP VIIRS at 01h10 showed no indication of a fire at Elandskraal.
- The first evidence of a fire at Elandskraal was at 06h03 on 7 June 2017, when the MSG geostationary satellite detected a thermal anomaly.
- Due to the coarse resolution of the MSG satellite image, a fire needs to be between 1 ha and 2 ha in size and a temperature of at least 700K before it will be detected.
- First evidence of the Kruisfontein fire detected by MSG was at 04h03. The known start time of the Kruisfontein fire was between 03h20 - 03h30, indicating a 33 - 43 minute delay before the MSG detection. This suggests a potential start time for the Elandskraal fire between 05h20 and 05h30.
- The Bushnell motion-sensing camera at Kooigoed captured evidence of the approaching fire at 06h48.
- A Rothermel fire spread model simulation initiated from the holdover fire location and based on average weather data between 05h00 and 05h17, estimated a time of arrival of the fire at Kooigoed at approximately 93 min after initialisation, suggesting a fire flare-up at 05h15
- Taking all the above-mentioned information into account, a probable time of ignition is estimated between 05h00 and 05h30.
- Topographic influences such as backdrafts or eddies could have potentially trapped the initial flaring fire until it grew large enough to escape the influence of the eddy effect, thus complicating more accurate estimates of time of flare-up of the fire.

Initial spread of the fire

- Damage to the croquet lawn and homestead (located 524 m south-east from the holdover fire) indicates a fire that approached from the northwest, burning and scorching the kikuyu lawn mostly on the north, north-eastern and north-western edges.
- Bushnell motion-sensing camera at Kooigoed (33.9628 S, 22.855 E) first photographs the fire approaching from the north-west. The time that the fire took to spread from the 1-2 ha active fire detection (06h03) to Kooigoed (06h48) is estimated at 45 minutes. The distance between these two points is approximately 1 433 m, and thus the mean rate of spread was calculated at 31.8 m/min.
- V-shaped patterns in the burned area indicate potential “spotting” of the fire which create new ignition points where burning embers may have landed after being transported vast distances by the strong winds.

Total area burned

A Sentinel-2 image of 14 June 2017 was used to map the total burned area of the Elandskraal and Kruisfontein fires and the estimated area burn was 9 440 ha excluding burned areas underneath tree canopies.

Based on the location and size of the holdover fire in relation to the final burn scar, the prevailing north-westerly berg wind conditions, as well as the direction from which the head fire propagated and burned into the croquet lawn, the conclusion can be made that the smouldering patch of vegetation observed by the drone footage on the 27 May 2017 and in the Sentinel-2 imagery was the most probable cause of the Elandskraal fire.

6 RECOMMENDATIONS

Holdover fires have the potential to flare-up under severe weather conditions with potentially devastating consequences, as was seen in the Knysna fire disaster. In order to reduce the risks of these events in future, the CSIR recommends the development of a system to calculate Lightning-Induced Fire Ignition Probability Index for South African conditions. Such a probability index will allow for the early detection of positive lightning strikes specifically in areas with very dry vegetation fuels and the subsequent detection of patches of smouldering and dying vegetation, which can be performed with satellite image time series data. AFIS currently assists fire managers by continuously monitoring weather conditions and alerting (via SMS and web-interface) to the existence of active fires. This service could be expanded to include fuel (vegetation) condition and lightning monitoring to calculate and map the Lightning-Induced Fire Ignition Probability. The automated monitoring of lightning-induced holdover fires could be incorporated into the operational AFIS system and combined with other relevant data to highlight risk to specific communities in near real-time. This would direct attention of firefighting authorities and local communities to the existence of a potential smouldering fires so that timely action can be taken to extinguish the fire before the fire flares-up. The SAWS lightning detection network needs to be expanded in order to improve lightning detection location accuracies, as well as more research into historical lightning occurrences and behaviour of lightning-induced holdover fires across South Africa.

The report also highlights the valuable contribution of airborne drones in investigating potential ignition sources in inaccessible areas. Such drone surveys can be guided by geospatial analysis of satellite data to identify specific, high-risk areas of interest and provide multi-temporal spatial context as demonstrated (retrospectively) in this report. There is little doubt that firefighting authorities will increase the operational use of drones for investigations and tactical firefighting in future.

Fire risk along the wildland-urban interface (WUI) of the fynbos biome can be calculated and mapped using the geospatial assessment procedure (or framework) previously demonstrated by the CSIR for specific study areas (Forsyth and Le Maitre 2015). We recommend that the risk assessment procedure be expanded to the entire fynbos biome (or all fire-prone biomes in the country) and augmented by including data of fuel type, fuel load (biomass), fuel moisture and burn history (time since last burn), all of which can already be derived from satellite imagery on an ongoing basis. The local landowners and government should be very well informed about fire risk along the WUI and share the responsibility for mitigating the risk of wildfires (Forsyth and Le Maitre 2015). To this end, fire risks should be continuously assessed, with risk maps being publicly accessible through web-based geographic information systems. Earth Observation and geospatial technologies are sufficiently mature to provide essential fire risk and other fire related information demonstrated in this report, however sufficient funding is required to take this technology beyond the "proof-of-concept" or "pilot" phases towards an operational service. The mitigation of the risk of inevitable wildfires in the fynbos biome, will therefore require (i) more research on the occurrence and behaviour of lightning-induced holdover fires, (ii) the development of a system to map the Lightning-Induced Fire Ignition Probability Index based on lightning strike data and satellite data, (iii) a system for mapping fire risk in WUI and for publicly disseminating these maps, (iv) broader communication of fire danger based on weather conditions, (v) sufficient support and funding to maintain these operational, public-good, fire information systems and finally, (vi) close collaboration between local landowners and government by means of fire protection associations to mitigate fire risk.

7 ACKNOWLEDGEMENTS

- The International Charter for Space and Major Disasters provided a wealth of near real-time satellite imagery that allowed for the detailed analysis of the Knysna fire disaster.

- The CSIR supported the production of this report and continue to support the operations of the Advanced Fire Information System (AFIS).

- The National Disaster Management Centre (NDMC) was instrumental in the activation of the International Charter for Space and Major Disasters.

- The Western Cape Disaster Management Centre (WCDMC) served as project manager for the Disaster Charter activation.

- Dr Coert Geldenhuys provided expert inputs during the analysis.

- The Elandskraal community provided access to the drone footage and Bushnell motion-sensing camera data.

- Mr Greg Forsyth and Dr David Le Maitre of the CSIR provided detailed review of the report.

- Mr Kobus Roux, Dr Quentin Williams and Dr Pravesh Debba of CSIR provided valuable inputs to the report.

- Prof. Emilio Chuvieco (University of Alcala, Spain) and Prof. Xavier Viegas (University of Coimbra, Portugal) provided detailed review of the report.

8 REFERENCES

Albini, F. A. (1976). Estimating wildfire behaviour and effects. USDA Forest Service. General Technical Report INT-30.

Anderson, H.E., Schuette, R.D., Mutch, R.W., 1978. Timelag and equilibrium moisture content of Ponderosa pine needles. USDA Forest Service, Intermountain Forest and Range Experiment Station, Research Paper INT-202, Ogden, UT.

Anderson, K. (2002) A Model to predict lightning-caused fire occurrence, Int. Journal of Wildland Fire, 11, 163 -172.

Bajocco, S. ,Dragoz, E. ,Gitas, I., Smiraglia, D., Salvati, L., Ricotta, C., 2015, Mapping Forest Fuels through Vegetation Phenology: The Role of Coarse-Resolution Satellite Time-Series, PLOS ONE, 10(3): e0119811. https://doi.org/10.1371/journal.pone.0119811

Bertschi, I., Yokelson, R. J., Ward, D. E., Babbitt, R. E., Susott, R. A., Goode, J. G., & Hao, W. M. (2003). Trace gas and particle emissions from fires in large diameter and belowground biomass fuels. Journal of Geophysical Research: Atmospheres, 108(D13), n/a-n/a. https://doi.org/10.1029/2002JD002100

Burgan, R. E., & Rothermel, R. C. (1984). Behave: Fire Behaviour Prediction and Fuel Modeling System - Fuel Subsystem. General Technical Report INT-167, Intermountain Forest and Range Experiment Station, United States Department of Agriculture, Forest Service, Ogden, Utah. https://doi.org/10.1017/CBO9781107415324.004

Calle, A., Casanova, J. L., & Romo, A. (2006). Fire detection and monitoring using MSG Spinning Enhanced Visible and Infrared Imager (SEVIRI) data. Journal of Geophysical Research: Biogeosciences, 111(4), 1–13. https://doi.org/10.1029/2005JG000116

Countryman, C. M., (1972). The fire environment concept. Berkeley, CA: USDA Forest Service, Pacific Southwest Forest and Range Experiment Station. 15 p.

Cummins, K. L. (1998). The US national lightning detection network and applications of cloud-to ground lightning data by electric power utilities. IEEE Transactions on Electromagnetic Compatibility [S.I.], v. 40, n. 4, p. 465-480.

Dozier, J., (1981). A Method for satellite identification of surface-temperature fields of subpixel resolution, Remote Sens. Environ., 11, 221 – 229.

Edwards D. (1984) Fire Regimes in the Biomes of South Africa. In: de Booysen P.V., Tainton N.M. (eds) Ecological Effects of Fire in South African Ecosystems. Ecological Studies (Analysis and Synthesis), vol 48. Springer, Berlin, Heidelberg

Finney, M. A., McHugh, C. W., Grenfell, I. C., Riley, K. L., & Short, K. C. (2011). A simulation of probabilistic wildfire risk components for the continental United States. Stochastic Environmental Research and Risk Assessment, 25(7), 973–1000. https://doi.org/10.1007/s00477-011-0462-z

Flannigan, M.D., and Vonder Haar, T.H. (1986) Forest fire monitoring using NOAA satellite AVHRR, Can. J. Forest Res., 16,975-982.

Flasse, S. P., and Ceccato, P., (1996) A contextual algorithm for AVHRR fire detection. Int. J. Remote Sens. 17(2), 419-424.

Forsyth, G.G. and LeMaitre, D.C. (2015) RISK TO COMMUNITIES AT THE WILDLAND-URBAN INTERFACE. Report No: CSIR/NRE/ECOS/ER/2015/0075/B, Natural Resources and the Environment, CSIR, Stellenbosch.

Forsyth G.G., Kruger F.J. and Le Maitre D.C. 2010. National Veldfire Risk Assessment: Analysis of exposure of social, economic and environmental assets to veldfire hazards in South Africa. Report No: CSIR /NRE/ECO/ER/2010/0023/C, Natural Resources and the Environment, CSIR, Stellenbosch.

Frandsen, W.H., (1997) Ignition probability of organic soil. Can. J. For. Res. 27: 1471-1477.

Fuquay, D. M., (1972) Lightning discharges that caused forest fires. J. Geophy. Res., 77, 2156-2158.

Fuquay, D.M., Baughman, R.G., Latham, D.J., (1979). A model for predicting lightning fire ignition in wildland fuel. USDA Forest Service. Intermountain Forest and Range Experiment Station, Research Paper INT-217, Ogden, UT.

Fuquay, D. M., (1982) Positive cloud-to ground lightning in summer thunderstorms. J. Geophys. Res., 87, 7131–7140.

Gallo, K.P. (1990) Satellite derived vegetation indices: A new climatic variable? Proceedings of the Symposium on Global Change Systems, Special Sessions on Climate Variations and Hydrology, 05- 09 February, Anaheim, California, Amer. Meteor. Soc., pp. 133-137.

Geldenhuys , C. J. (1982) The Management of the Southern Cape Forests, South African Forestry Journal. Vol. 121 , 4-10.

Geldenhuys, C. J. (1994). Bergwind fires and the location pattern of forest patches in the southern Cape landscape, South Africa. Journal of Biogeography, 21(1), 49–62. https://doi.org/10.2307/2845603

Giglio, L., Kendall, J. D., & Mack, R. (2003). A multi-year fire data set for the tropics derived from the TRMM VIRS. International Journal of Remote Sensing 87, 273 - 282.

Gill T. (2008). Initial steps in the development of a comprehensive lightning climatology of South Africa. MSc thesis, Johannesburg, University of the Witwatersrand.

Granger, J. E., (1984). Fire in forest. In: P. de V. Booysen & N. M. Tainton (eds.). Ecological effects of fire in South African ecosystems, pp. 177–197. Springer-Verlag, New York.

Goetz, S.J., Fiske, G.J., Bunn, A.G., (2006). Using satellite time-series data sets to analyze fire disturbance and forest recovery across Canada. Remote Sensing of Environment, 101, 352–365.

Grant, M. D., McKechnie, I. S., Jandrell, I. R., & Nixon, K. J. (2011). Probabilistic interpretation of LDN confidence ellipses with reference to forensic applications. 2011 7th Asia-Pacific International Conference on Lightning, APL2011, 750–754. https://doi.org/10.1109/APL.2011.6110227

Holben, B.N. (1986) Characteristics of maximum-value composite images from temporal AVHRR data. Int J Remote Sensing 7: 1417-1434.

Horne, I. P. (1981). The frequency of fires in the Groot Swartberg mountain catchment area, Cape Province. S. Afr. For. J. 118: 56-50.

Huete, A., Didan, K., Miura, T., Rodriguez, E.P., Gao, X., Ferreira, L.G. (2002). Overview of the radiometric and biophysical performance of the MODIS Vegetation Indices. Remote Sens. Environment, 83, 195–213.

Jiang, Z., Huete, A. R., Didan, K. & Miura T. (2008). Development of a two-band Enhanced Vegetation Index without a blue band, Remote Sensing of Environment, 112(10), 3833-3845, doi:10.1016/j.rse.2008.06.006.

Latham, D.J.; Schlieter, J.A., (1989) Ignition probabilities of wildland fuels based on simulated lightning discharges. Research Paper Intermountain Research Station, USDA Forest Service (INT-411): i + 16 pp.

Laneve, G., & Cadau, E. (2006). SEVIRI / MSG sensor early fire detection performances assessment, (December), 4–6.

Martin, J., & Hillen, T. (2016). The spotting distribution of wildfires. Applied Sciences, 6(6), 177. https://doi.org/10.3390/app6060177

Matson, M., and J. Dozier, (1981). Identification of subresolution high temperature sources using a thermal IR sensor. Photo. Engr. and Rem. Sens. 47,1311-1318.

Meikle, S., & Heine, J. (1987). A fire index system for the Transvaal lowveld and adjoining escarpment areas. South African Forestry Journal, 143, 55 - 57.

Moritz, M. A., Morais M.E., Summerell, L.A., Carlson J. M. & Doyle, J. (2005). Wildfires, complexity, and highly optimized tolerance, Proceedings of the National Academy of Sciences, 102 (50) 17912-17917 https://doi.org/10.1073/pnas.0508985102

le Roux, P.J. 1979. The occurrence of fires in the southern Cape fynbos. Paper presented at the Conference on Terrestrial Ecology of the Southern Cape, George. pp 13 (cited in Edwards, 1984).

Lasaponara, R., Cuomo, V., Macchiato, MF., (2003). A self-adaptive algorithm based on AVHRR multitemporal data analysis for small active fire detection INTERNATIONAL JOURNAL OF REMOTE SENSING Vol 24, 1723-1749 2003.

Liu H.Q., Huete A.R. (1995). A feedback based modification of the NDVI to minimize canopy background and atmospheric noise. IEEE Transactions on Geoscience and Remote Sensing. 33:457–465

Lopes, A.M.G., Cruz, M.G. and Viegas, D.X., (2002). FireStation – an integrated software system for the numerical simulation of fire spread on complex topography. Environmental Modelling & Software, 17, 269-285.

Rein, G., Garcia, J., Simeoni, A., Tihay, V., & Ferrat, L. (2008). Smouldering natural fires: Comparison of burning dynamics in boreal peat and Mediterranean humus. WIT Transactions on Ecology and the Environment, 119, 183–192. https://doi.org/10.2495/FIVA080191

Rothermel, R. C. (1972). A mathematical model for predicting fire spread in wild land fuels. USDA Forest Service Research Paper INT-115.

Shindo, T. and Uman, M.U., (1989). Continuing current in negative cloud to-ground lightning. J. Geophys. Res. 94, 5189-5198.

Sullivan Andrew L. (2009) Wildland surface fire spread modelling, 1990–2007. 3: Simulation and mathematical analogue models. International Journal of Wildland Fire, 18, 387-403. https://doi.org/10.1071/WF06144

Tucker, C.J. (1979) Red and Photographic Infrared Linear Combinations for Monitoring Vegetation. Remote Sens Environment 8: 127-150.

Tucker, C.J. (1996) History of the Use of AVHRR Data for Land Applications. In Advances in the Use of NOAA AVHRR Data for Land Applications, ed. G. D'Souza, A.L. Belward, and J. Malingreau, 1-19. Dordrecht: Kluwer Academic Publishers.

Tyson, P. D. (1964). Berg winds of South Africa. Weather, 19(1), 7–11. https://doi.org/10.1002/j.1477-8696.1964.tb02714.x

Vaisala User Guide: https://www.vaisala.com/sites/default/files/documents/8.Bourscheidt-Using%20the%20Gaussian.pdf

van Wilgen B.W. (1982). Some effects of post-fire age on the above-ground biomass of fynbos (macchia) vegetation in South Africa. J. Ecol. 70, 217–225.

van Wilgen, B.W. (1984a). Fire climates in the southern and western Cape Province and their potential use in fire control and management. South African Journal of Science 80, 358–362.

van Wilgen, B.W. (1984b). Adaptation of the United States fire danger rating system to fynbos conditions. I: A fuel model for fire danger rating in the fynbos biome. South African Forestry Journal 129, 61-65.

van Wilgen, B. W., Le Maitre, D. C., & Kruger, F. J. (1985). Fire Behaviour in South African Fynbos (Macchia) Vegetation and Predictions from Rothermel's Fire Model. Journal of Applied Ecology, 22, 207–216.

Vlok, J. H. J., Euston-Brown, D. I. W., & Wolf, T. (2008). A vegetation map for the Garden Route Initiative. Unpublished 1:50 000 maps and report supported by CAPE FSP task team. Prepared by Regalis Environmental Services for the Garden Route Initiative.

Von Breitenbach, F. 1974. Southern Cape forests and trees. Government Printers, Pretoria. R.S.A. 328 pp.

Wotton, B. M., Logan K. A. and McAlpine, R. S., (2005). Climate change and the future fire environment in Ontario: fire occurrence and fire management impacts Ontario Ministry of Natural Resources Climate Research Report CCRR-01 32

9 GLOSSARY

Active fire detection	Actively burning fires are detected on satellite imagery on the basis of thermal anomalies it produces. The algorithms compare the temperature of a potential fire with the temperature of the land cover around it; if the difference in temperature is above a given threshold, the potential fire is confirmed as an active fire or "hot spot."
Advanced Fire Information System (AFIS)	AFIS provides information on current and historical fires detected by sensors on Earth observation satellites, e.g. NASA MODIS, EUMETSAT MSG, GOES, NPP, etc. covering multiple regions across the globe. The system provides monitoring of active fires on a web-based map and delivers near real-time alerts to registered users when a fire is detected within their specified areas of interest via email, SMS, XMPP, etc.
Advanced Very High Resolution Radiometer (AVHRR)	A broad-band, four or five channel (depending on the model) scanner, sensing in the visible, near-infrared, and thermal infrared portions of the electromagnetic spectrum. This sensor is carried on the NOAA's Polar Orbiting Environmental Satellites (POES). AVHRR is an integrated system that combines automated fire detection algorithms with human interpretation to identify fire activity and smoke.
Anticyclonic weather	A large-scale weather phenomenon characterized by circulation of winds around a central region of high atmospheric pressure, moving counter clockwise in the Southern Hemisphere. In summer, anticyclones bring dry, hot weather.
Atmospheric attenuation	Absorption of electromagnetic waves in the atmosphere according to wavelength.
Atmospheric effects	Electromagnetic radiation can be absorbed or scattered by the constituent particles of the atmosphere as it travels through the atmosphere.
Bushnell motion-sensing camera	Automated wildfire sensing system based on using visible light, standard security style video cameras for sensors and pattern recognition software as the detection and fire presence signalling system
Backdraft	Instantaneous explosion or rapid burning of superheated gases that occurs when oxygen is introduced into an oxygen-depleted confined space.
Berg wind	A hot dry wind in South Africa blowing from the plateau down to the coast

Brightness temperature	A measurement of the radiance of the microwave radiation traveling upward from the top of the atmosphere to the satellite, expressed in units of the temperature of an equivalent black body
Burned area	Areas characterized by deposits of charcoal and ash, removal of vegetation, and alteration of the vegetation structure
Canopy structure	Vegetation layers in forests are generally distinguished as forest floor (root and soil layers), herbaceous, shrub, understory and canopy layers. These vegetation layers are primarily determined by the height of their individual plants with canopy (tree) structure as the highest.
Chaparral Fuel Type	Properties embedded within this fuel model adequately represent the fynbos vegetation characteristics found in South Africa
Combustion	Combustion involves several phases (pre-combustion, flaming, smouldering, and glowing) as a fire advances through fuel, generating heat that produces a convection column that vertically lifts by-product gases, vapours, and particulates (smoke). In the pre-combustion (or pre-heating) phase, fuel elements ahead of the fire are heated, causing fuels to dry. Heat induces thermal decomposition (pyrolysis) of some components of woody fuels, causing release of combustible organic gases and vapours.
Convection	In meteorology, convection is the predominantly vertical movement of warmed air. Heated air and gases rise above burning fuels into tree canopies, scorching and preheating them; smoke plumes are convective
Copernicus	Copernicus is the European Union's Earth Observation Programme, it offers information services based on satellite Earth Observation and in situ (non-space) data. The Sentinel satellites are part of this programme
Council for Scientific and Industrial Research (CSIR)	The Council for Scientific and Industrial Research (CSIR) is South Africa's scientific research and development organisation. The CSIR contract R&D portfolio aims to enable clear understanding of national imperatives and the needs of industry to optimise the impact of the CSIR's R&D outputs.
Curing	A process that leads to the reduction in moisture content of dead vegetation. This usually causes the vegetation to turn brown in appearance.
Day/Night Band	Products from the Visible Infrared Imaging Radiometer Suite (VIIRS) night-time sensor (also called the Day/Night Band, or DNB), which are available generally within three hours of an overflight of the joint NASA/NOAA Suomi National Polar-orbiting Partnership (Suomi-NPP) satellite.

Digital Elevation Model (DEM)	A specialized database that represents a 3D model of topography / relief of the earth's surface
Drone	Drones are formally known as unmanned aerial vehicles (UAVs) or unmanned aircraft systems (UASes). The aircrafts may be remotely controlled or can fly autonomously through software-controlled flight plans in their embedded systems working in conjunction with on-board sensors and GPS.
Dry or Scrub woodland forest	Very dry scrub forest is characterised by thorny undergrowth (sometimes dense), some thorny under-canopy tree species, low canopy, gnarled tree trunks, and forest floor generally dry.
Earth observation satellites	Satellites specifically designed for Earth observation from orbit, intended for non-military uses such as environmental monitoring, meteorology, map making etc.
Eddies	A movement in a stream of air, water, or other fluid in which the current doubles back on itself causing a miniature whirlwind or whirlpool. Eddy winds form around large objects and along tree lines. It can strongly influence fire behaviour at the edge of stands, open fields or along roads.
Electromagnetic spectrum	The range of energy which contains parts or "bands" such as the visible, infrared, ultraviolet, microwave (radar), gamma ray, x-ray, radio, and which travels at the speed of light. Different parts of the electromagnetic spectrum have different wavelengths and frequencies.
Enhanced Vegetation Index (EVI)	An 'optimized' vegetation index designed to enhance the vegetation signal with improved sensitivity in high biomass regions. EVI is more responsive to canopy structural variations, including leaf area index (LAI), canopy type, plant physiognomy, plant phenology, canopy architecture and plant stress
European Organisation for the Exploitation of Meteorological Satellites (EUMETSAT)	EUMETSAT is an intergovernmental organisation with a total of 30 European Member States, with the primary objective to establish, maintain and exploit European systems of operational meteorological satellites. EUMETSAT is responsible for the launch and operation of the satellites and for delivering satellite data to end-users as well as contributing to the operational monitoring of climate and the detection of global climate changes.
European Space Agency (ESA)	The agency is the coordinating entity for European civilian space activities. With 22 member states, its headquarters is in Paris, and it also has several centres scattered in several European countries.
Fine fuel	Fast-drying fuels, generally with a comparatively high surface area-to-volume ratio, which are less than 6 mm in diameter and have a time

	lag of one hour or less. These fuels readily ignite and are rapidly consumed by fire when dry.
Fire behaviour model	A method or tool used to forecast future behaviour of a fire. Indicators such as Total Fuel Consumption (TFC), Rate of Spread (ROS) and Head Fire Intensity (HFI) are calculated in fire behaviour models. This calculation is derived from basic physical models and provides physically understandable quantities expressed in units.
Fire behaviour	The manner in which a fire reacts to the variables of fuel, weather and topography. Different types of fire behaviour include, smouldering, creeping, running, spotting, torching and crowning fires.
Fire danger	A general term used to express an assessment factors of the fire environment that determine the ease of ignition, rate of spread, difficulty of control, and impact fire danger (or potential). It is often expressed as an index but cannot be measured directly. It is inferred by measuring weather components such as temperature, relative humidity, rainfall and wind speed.
Fire danger index (FDI)	A relative number denoting an evaluation of rate of spread, or suppression difficulty for specific combinations of temperature, relative humidity, drought effects and wind speed. The values may range from 1 to 100.
Fire danger rating	An evaluation of rate of spread, or suppression difficulty for specific combinations of temperature, relative humidity, drought effects and wind speed. Rated as low, moderate, high, very high or extreme.
Fire spread	The movement of a fire through available fuels arranged across the landscape.
Fire Weather	Fire weather refers to meteorological conditions that influence fire ignition, behaviour, and suppression.
Fire weather index (FWI)	The Canadian Forest Fire Weather Index (FWI) system consists of six components that account for the effects of fuel moisture and wind on fire behaviour. It is numeric rating of fire intensity based on meteorological conditions. It combines the Initial Spread Index and the Buildup Index and is suitable as a general index of fire danger. FWI is used globally.
Flank fire	Part of a fire's perimeter that are roughly parallel to the main direction of spread.
Flare-up	A fire bursting (as of a smouldering fire) into flame causing acceleration in rate of spread or intensification of the fire
Fuel	Fuels are vegetation: live, dead, or decomposed. Any material such as grass, leaf litter and live vegetation which can be ignited and sustains a

	fire. Fuel is usually measured in tonnes per hectare. Characteristics important for predicting fire behaviour include compactness, loading, horizontal continuity, vertical arrangement, chemical content, size and shape, and moisture content.
Fuel Bed	Commonly used to describe the fuel composition in natural settings, referring to specific loading, depth and particle size
Fuel Model	Simulated fuel complex (or combination of vegetation types) for which all fuel descriptors required for the solution of a mathematical rate of spread model have been specified.
Fuel moisture content	The water content of a fuel expressed as a percent of the oven dry weight of the fuel particle
Fuel Type	An association of fuel elements of a distinctive plant species, form, size, arrangement, or other characteristics that will cause a predictable rate of fire spread or difficulty of control under specified weather conditions.
Gaseous fuel	Fire occurs whenever combustible fuel in the presence of oxygen at an extremely high temperature becomes gas. Flames are the visual indicator of the heated gas.
Gas-phase ignition	In the first phase (pre-ignition) of combustion fuels ahead of the fire are pre-heated by convection and radiation which cause drying of fuel (~100°C) and volatiles to evaporate into a gas phase. This is followed by gas-phase ignition when oxidisation occurs and flames become visible.
Geolocation	Geolocation is the identification or estimation of the real-world geographic location of an object.
Geostationary orbit	Describes an orbit in which a satellite appears stationary with respect to the rotating Earth. The satellite travels around the Earth in the same direction, at an altitude of approximately 35,790 km because that produces an orbital period equal to the period of rotation of the Earth (actually 23 hours, 56 minutes, 04.09 seconds).
Ground Fuel	All combustible materials below the surface litter, including duff, tree or shrub roots, wood, peat, and sawdust that normally support a glowing combustion without flame.
Head of a Fire	The leading part of an advancing wildfire at a particular point in time. The head fire will usually exhibit the highest level of fire activity and the fastest rate of spread of any part of the fire.

Holdover fire	Fire started by lightning strikes that go underground and erupt several days or weeks later from wind or hot, dry conditions. Holdover fires are slow, low-temperature, flameless fires that spread both horizontally and vertically through organic layers or roots depending on the vegetation and soil structure. Once ignited they are extremely difficult to extinguish and can persist for long periods of time
Ignition	The beginning of flame production or smouldering combustion; the starting of a fire
Image	Pictorial representation of a scene recorded by a remote sensing system. Although image is a general term, it is commonly restricted to representations acquired by non-photographic methods.
Infrared (IR)	Infrared region of the electromagnetic spectrum that includes wavelengths from 0.7 µm to 1 mm.
International Charter for Space and Major Disasters	The International Charter "Space and Major Disasters" is a non-binding charter which provides for the charitable and humanitarian re-tasked acquisition of and transmission of space satellite data to relief organizations in the event of major disasters. The International Charter aims at providing a unified system of space data acquisition and delivery to those affected by natural or man-made disasters through Authorized Users
Leaf area index (LAI)	An important biophysical parameter in ecological modelling and characterization of plant canopies. It is a dimensionless ratio of leaf area per unit ground area. LAI controls many ecological processes like photosynthesis, evaporation and transpiration.
Litter	Top layer of the forest, scrubland, or grassland floor, directly above the fermentation layer, composed of loose debris of dead sticks, branches, twigs, and recently fallen leaves or needles, little altered in structure by decomposition
Long continuing current (LCC)	A continuous electric charge lasting longer than 40 ms
Long wave infrared (LWIR)	See “Thermal (IR)”
Low resolution	Satellite data with low and medium resolution are characterized by spatial resolution at more than 1 km and hundreds of meters, respectively. Due to the wide swath of these satellites the data with daily or a-few-day frequency are guaranteed.

Lowveld Fire Danger Index (LFDI)	Fire danger index currently being used in parts of South Africa. The calculation of the Burning index (BI) uses a simple nomogram using temperature and relative humidity or computer programs. The burning index it is then adjusted for wind by adding a value according to the prevailing wind conditions at 14h00.
Meteosat Second Generation (MSG)	The MSG geostationary satellites carry the Scanning Enhanced Visible and InfraRed Imager (SEVIRI). These advanced weather satellites are operated as a two-satellite system returning detailed imagery of Europe and Africa every 15 minutes, for operational use by meteorologists. Fire detection takes place at a 4 km spatial resolution in the nadir point in the [3.5–4.0 µm] spectral region.
Mid-infrared (MIR)	The range of electromagnetic wavelengths from 3 to 15 µm dominated by emission of thermally generated radiation from materials; also known as thermal infrared.
Mid-wave infrared (MWIR)	See "Mid-infrared (MIR)"
Minimum detectable fire size	Minimum detectable fire size is a function of many different variables (scan angle, biome, sun position, land surface temperature, cloud cover, amount of smoke and wind direction, etc.), so the precise value will vary slightly with these conditions
Moderate Resolution Imaging Spectroradiometer (MODIS)	The MODIS sensor is on both the Terra and Aqua satellites, and together with the National Polar-orbiting Partnership (NPP) Visible Infrared Imaging Radiometer Suite (VIIRS) sensor on the SUOMI satellite. The instruments capture data in 36 spectral bands ranging in wavelength from 0.4 µm to 14.4 µm and at varying spatial resolutions (2 bands at 250 m, 5 bands at 500 m and 29 bands at 1 km). Together the instruments image the entire Earth every 1 to 2 days. The MODIS active fire product detects fires in 1 km pixels that are burning at the time of overpass under relatively cloud-free conditions using a contextual algorithm. Burn area mapping is produces on a monthly basis.
National Aeronautics and Space Administration (NASA)	The National Aeronautics and Space Administration is an independent agency of the United States federal government responsible for the civilian space program, as well as aeronautics and aerospace research
National Disaster Management Centre (NDMC)	This centre is established in terms of Section 8 of the Disaster Management Act, 2002 (Act No 57 of 2002) (DMA). The objective of the National Centre is to promote an integrated and co-ordinated system of disaster management, with special emphasis on prevention and mitigation, by national, provincial and municipal organs of state, statutory functionaries, other role-players involved in disaster management and communities.

National Integrated Water Information System (NIWIS)	The Department of Water and Sanitation launched the National Integrated Water Information System. The primary objective of NIWIS is to provide information to water management institutions, water users, the public, researchers, scientists, decision makers and those interested in getting a deeper understanding and knowledge of the water status in the country.
National Oceanic and Atmospheric Administration (NOAA)	A United States scientific agency that focuses on the conditions of the oceans and the atmosphere. NOAA provides timely access to global environmental data from satellites and other sources to monitor and warn of dangerous weather and conducts research to provide understanding and improve stewardship of the environment
National Polar-orbiting Partnership (NPP)	The Suomi National Polar-orbiting Partnership or Suomi NPP, previously known as the National Polar-orbiting Operational Environmental Satellite (NPOES) Preparatory Project (NPP), is a weather satellite operated by NOAA. Originally intended as a pathfinder for the NPOESS program.
Near infrared (NIR)	The shorter wavelength range of the infrared region of the electromagnetic spectrum, from 0.7 to 2.5 µm. It is often divided into very-near infrared (VNIR) covering the range accessible to photographic emulsions (0.7 to 1.0 m), and the short-wavelength infrared (SWIR) covering the remainder of the NIR atmospheric window from 1.0 to 2.5 µm.
Normalised Difference Vegetation Index (NDVI)	An index calculated from reflectance measured in the visible and near infrared channels. It is related to the fraction of photosynthetically active radiation (fPAR). The chlorophyll (green pigment) absorbs incoming radiation in the visible band, while the leaf structure and water content is responsible for a very high reflectance in the near-infrared region of the spectrum. NDVI has been correlated to a variety of vegetation parameters, including quantity, productivity, biomass, vegetation condition and plant stress.
Orbit	The path traced by a satellite as it passes around a planet.
Organic layer	The top, organic layer of soil, made up mostly of leaf litter and humus (decomposed organic matter).
Photosynthetic activity	Photosynthesis is a process used by plants and other organisms to convert light energy into chemical energy. Photosynthetic activity is defined as a function of leaf area development, photosynthetic rate, and source-sink ratio responses
Photosynthetically active radiation (PAR)	Photosynthetically active radiation (PAR) is the spectral range from 400-700nm that is used by plants in photosynthesis. The fraction of PAR (fPAR) is a parameter used in remote sensing and in ecosystem modelling that signifies the portion of PAR used by plants.

Pixel	Pixel is short for picture element. It is the ground area corresponding to a single element and the smallest unit in a digital image. A satellite image is made up of a matrix of many pixels, each having its own digital value.
Pixel saturation	The incident light at a pixel causes one of the colour channels of the camera sensor to respond at its maximum value, can produce undesirable artefacts in digital colour images
Planck's law	An expression for the variation of emittance of a blackbody at a particular temperature as a function of wavelength.
Plant physiognomy	Physiognomy is a combination of the external appearance of vegetation, its vertical structure, and the growth forms of the dominant taxa.
Polar orbit	An orbit with an orbital inclination of near 90 degrees where the satellite ground track will cross both polar regions once during each orbit. The term is used to describe the near-polar orbits of spacecraft such as the USA's NOAA/TIROS and Landsat satellites.
Positive lightning strike	Lightning is an electrical discharge caused by imbalances between storm clouds and the ground, or within the clouds themselves. Positive strikes originates in the upper levels of a storm and its electric field typically is much stronger than a negative strike. Its flash duration is longer, and its peak charge and potential can be ten times greater than a negative. Voltage and current of positive bolts are 10 times more powerful than the typical negative strike. Positive strikes are usually the cause of forest fires, house fires and damage to planes and power grids.
Prefrontal weather	High temperatures, strong dry winds, possible thunderstorms, and rapidly shifting wind direction is associated with prefrontal troughs.
Preheating	Preliminary phase of combustion where fuels ahead of an advancing fire are heated and dried. Fuel temperatures can be raised either by the advancing fire and/or by weather (i.e. solar radiation, aspect).
Provincial Disaster Management Centre (PDMC)	Each province in South Africa has a PDMC aimed at ensuring an integrated and uniform approach to disaster management by all provincial organs of state, provincial statutory functionaries, non-governmental organisations and the private sector.
Radiance	Light or heat emitted or reflected by an object.
Radiant energy	Energy that is transferred by electromagnetic radiation, such as light, X-rays, gamma rays, and thermal radiation, which may be described in terms of either discrete packets of energy, called photons, or continuous electromagnetic waves.

Radiation	Heat radiated from a feature for example a flaming front that pre-heats grass, shrub, and tree fuels, causing the flaming front to move along
Rate of spread (ROS)	The speed with which a fire moves in a horizontal direction across the landscape at a specified part of the fire perimeter.
Reflectance	The measure of the proportion of light or other radiation striking a surface which is reflected off it. Spectral reflectance is the reflectance measured within a specific wavelength interval.
Relative Humidity (Rh)	The ratio of the amount of moisture in the air, to the maximum amount of moisture that air would contain if it were saturated.
Remote sensing	The action of collecting images or other forms of data about the surface of the Earth, from measurements made at some distance above the Earth, processing these data and analysing them.
Rothermel fire spread model	The Rothermel (1972) fire spread model is one of the most used models to simulate the forward rate of spread (ROS) at the head of a surface fire, and is the primary fire spread model of many fire prediction systems
Satellite	A remote sensing satellite carries one or more instruments for recording images of the Earth, which are transmitted to a receiving station using radio waves
Saturation	Saturation is the condition where energy flux exceeds the sensitivity range of a detector.
Scanning Enhanced Visible and InfraRed Imager (SEVIRI)	The SEVIRI sensor, on board the Meteosat Second Generation (MSG) geostationary satellite, is the only space borne sensor providing five and 15-minute observations of Europe and Africa in 12 spectral channels, including a short-wave infrared band sensitive to fire radiative temperature
Sensor	A sensor is the device that records a remote sensing image, much like a camera.
Sentinel Playground	A web application for browsing, analysis and evaluation of Sentinel-2 imagery. Sentinel Playground utilises Sentinel Hub technology to enable easy-to-use discovery of full-resolution Sentinel-2 imagery, along with access to the EO data products.
Sentinel-2	Sentinel-2 is an Earth observation mission developed by ESA as part of the Copernicus Programme to perform terrestrial observations in support of services such as forest monitoring, land cover changes detection, and natural disaster management. It consists of two identical satellites Sentinel-2A and Sentinel-2B

Short-wave infrared (SWIR)	Short-wave infrared (SWIR) light is typically defined as light in the 0.9 – 1.7µm wavelength range. Imaging systems using the SWIR wavelength bands offer unique remote sensing capabilities, such as material detection and smoke penetration.
Shuttle Radar Topography Mission (SRTM)	The Shuttle Radar Topography Mission (SRTM) is an international research effort that obtained digital elevation models on a near-global scale from 56° S to 60° N, to generate the most complete high-resolution digital topographic database of Earth prior to the release of the ASTER GDEM in 2009.
Sleeper fire	See "holdover" fire
Smouldering Fire	Low intensity combustion with no flame and little or no fire spread. i.e. a fire burning without flame and barely spreading.
South African Lightning Detection Network (SALDN)	SAWS purchased a state-of-the-art lightning detection network from Vaisala in 2005, making South Africa one of only three countries in the southern hemisphere to operate such a network. This network provides information on lightning in thunderstorms, lightning impact on electrical distributions and populates a database on how lightning influences humans and animals. It also provides lightning information to the public.
South African National Parks (SANParks)	SANParks manages a system of parks which represents the indigenous fauna, flora, landscapes and associated cultural heritage of South Africa
South African Weather Service (SAWS)	The South African Weather Service was established in accordance with the South African Weather Service Act (Act No 8 of 2001). Its vision is to be the foremost provider of relevant services in respect of weather, climate and related products, which contribute to sustainable development in South Africa and the African continent
Southern Cape Afrotemperate Forests	Southern Afrotemperate Forest (the Southern Cape Forests) is a kind of tall, shady, multi-layered indigenous South African forest. This is the main forest-type in the south-western part of South Africa, naturally extending from the Cape Peninsula in the west, as far as Port Elizabeth in the east. In this range (apart from the massive Knysna-Tsitsikamma forest complex), it usually occurs in small forest pockets, surrounded by fynbos vegetation.
Southern Cape Fire Protection Association (SCFPA)	A registered Non Profit Company, which operates in an area from Witsand, along the Breederiver, North to the Swartberge – all along the Swartberge to the East at Willowmore and down South, towards Plettenberg Bay (EDEN Districts Municipality) as well as in the Eastern Cape, the Tsitsikamma, Langkloof and Baviaanskloof. ± 4 million Hectare area of responsibility. Its integrated fire management strategy

	aims to eliminate the impact of veld fires on the environment and communities.
Spectral reflectance	Reflectance of electromagnetic energy at specified wavelength intervals.
Spot fire	Isolated fire started ahead of the main fire by sparks, embers or other ignited material, sometimes to a distance of several kilometres
Spotting	Behaviour of a fire producing sparks or embers that are carried by the wind and start new fires beyond the zone of direct ignition by the main fire.
Surface Fuels	Loose surface litter on the soil surface, normally consisting of fallen leaves or needles, twigs, bark, cones, and small branches that have not yet decayed enough to lose their identity; also grasses, forbs, low and medium shrubs, tree seedlings, heavier branch wood, downed logs, and stumps interspersed with or partially replacing the litter.
Temperature	The measure of molecular motion or the degree of heat of a substance. It is measured on an arbitrary scale from absolute zero, where the molecules theoretically stop moving. It is also the degree of hotness or coldness. In surface observations, it refers primarily to the free air or ambient temperature close to the surface of the earth.
Thermal (IR)	Phrase used to describe the middle wavelength ranges in the infrared portion of the electromagnetic spectrum. Ranging between 3 µm and 20 µm, most remote sensing applications utilize the 8- to 14 µm range. This is emitted (radiant) energy whereas other infrared (near infrared) is reflected energy.
Thermodynamics	Science of the relationship between heat, work, temperature, and energy. In broad terms, thermodynamics deals with the transfer of energy from one place to another and from one form to another.
Time series	A series of values of a quantity obtained at successive times, often with equal intervals between them
Topography	Configuration (relief) of the land surface e.g. mountains
United States Geological Survey (USGS)	A scientific agency of the United States government. It provides reliable scientific information to describe and understand the Earth; minimize loss of life and property from natural disasters; manage water, biological, energy, and mineral resources; and enhance and protect our quality of life. NASA develops remote sensing instruments and the spacecraft, then launches and validates the performance of the instruments and satellites. The USGS then assumes ownership and operation of the satellites, in addition to managing all ground reception.

Vegetation condition	Stage of growth or degree of flammability of vegetation that forms part of a fuel complex. This will be dependent upon time of year, amount of curing and weather conditions.
Vegetation index	An index is an indicator that describes the greenness — the relative density and health of vegetation — for each picture element, or pixel, in a satellite image. Vegetation condition is based on differences in the amount of visible and near-infrared light reflected from plants on Earth's surface. A vegetation index is a gauge of plant health, productivity, and density. The most widely used are the Normalized Difference Vegetation Index (NDVI) and Enhanced Vegetation Index (EVI).
Visible Infrared Imaging Radiometer Suite (VIIRS)	The Visible Infrared Imaging Radiometer Suite (VIIRS) instrument is a component of the Suomi National Polar-orbiting Partnership (NPP) satellite. VIIRS data is used to measure cloud and aerosol properties, ocean colour, sea and land surface temperature, ice motion and temperature, fires, and Earth's albedo.
Visible light	The portion of the electromagnetic spectrum that is visible to the human eye. Electromagnetic radiation in this range of wavelengths is called visible light or simply light. A typical human eye will respond to wavelengths from about 390 to 700 nm.
Visual analysis	The process of examining an image and manually identifying the features in that image. This method can be highly reliable and a wide variety of features can be identified. The process is time consuming and requires a skilled analyst
Western Cape Disaster Management Centre (WCDMC)	The Provincial Disaster Management Centre (PDMC) in the Western Cape that provides a single environment where all disaster management activities can be planned for and coordinated in an integrated manner.
Wildland-urban Interface (WUI)	The wildland-urban interface (WUI), is defined as the area where structures and other human development meet or intermingle with undeveloped wildland. The expansion of the WUI in recent decades has significant implications for wildfire management and impact.
Wind direction	The direction from which the wind is blowing. It is reported with reference to true north, or 360 degrees on the compass, and expressed to the nearest 10 degrees.
Wind speed	The rate of the motion of the air on a unit of time.
WorldView-3	WorldView-3 is a commercial Earth observation satellite owned by DigitalGlobe. It collects data in Panchromatic and Multispectral bands, eight-band short-wave infrared (SWIR) and 12 band CAVIS (Clouds,

	Aerosols, Water Vapour, Ice, Snow) imagery. The spatial resolution is the highest level of detail commercially available from satellite.